

Article

Amelioration of Alcoholic Liver Disease by Activating PXR-Cytochrome P450s Axis with Blackberry Extract

Ting Xiao ^{1,2}, Zhenghong Guo ^{3,*}, Min Fu ², Jiaoyan Huang ², Xiaowei Wang ², Yuqing Zhao ⁴, Ling Tao ^{1,2} and Xiangchun Shen ^{1,2,*}

¹ The State Key Laboratory of Functions and Applications of Medicinal Plants, The Department of Pharmaceutic Preparation of Chinese Medicine, The High Educational Key Laboratory of Guizhou Province for Natural Medicinal Pharmacology and Druggability, School of Pharmaceutical Sciences, Guizhou Medical University, Guiyang 550025, China

² The Key Laboratory of Optimal Utilization of Natural Medicine Resources, School of Pharmaceutical Sciences, Guizhou Medical University, University Town, Gui'an New District, Guiyang 550025, China

³ School of Pharmacy, Guizhou University of Traditional Chinese Medicine, Guiyang 550025, China

⁴ School of Functional Food and Wine, Shenyang Pharmaceutical University, Shenyang 110016, China

* Correspondence: sxc@gmc.edu.cn (X.S.); guo_zhenghong@163.com (Z.G.)

Abstract: Blackberry is widely used in diets for its rich biological phytochemicals and health benefits. However, the relationship between the effect of blackberry extract (BBE) on ameliorating alcoholic liver disease (ALD) and the PXR-Cytochrome P450s axis *in vivo* and *in vitro* is unknown. In this study, 50% and 30% ethanol by gavage were used to establish acute and subacute ALD. Male mice were intragastrically administered BBE with 25, 50, and 100 mg/kg BW in the treatment groups. In the experiment, samples were collected, and related indices and histopathological observation were measured. In addition, the potential mechanism was predicted by network and docking studies, which were verified by qRT-PCR analysis, the detection of apoptosis, the measurement of mitochondrial membrane potential, the detection of ROS levels, and Western blotting in liver tissues and HepG2 cells. The acute and subacute ALD experiments indicated BBE ameliorated liver indices, AST, ALT, SOD, and MDA in serum, and the histopathology changed, as observed via H&E, Sirius red, and oil red O staining. The potential mechanism was predicted by network and docking studies, which were verified by experiments. Western blotting suggested BBE reduced the protein expression of NF- κ B, TGF- β , IL-6, and α -SMA, and enhanced PXR and CAR in livers. In addition, qRT-PCR showed BBE significantly elevated the mRNA levels of *PXR*, *CAR*, *CYP3A25*, *CYP3A11*, and *CYP2B10*. In the experiment of the ethanol-induced apoptosis of HepG2 cells, BBE reduced the apoptosis of HepG2 cells by boosting mitochondrial membrane potential, reducing the apoptotic rate and ROS content, lessening the expression of Bax, and inducing the expression of PXR. For the first time, this study demonstrated BBE's preventive effects on ALD, which are associated with the antioxidation and stimulation of the PXR-Cytochrome P450s axis. In addition, BBE is available as a nutritional agent.

Keywords: blackberry; PXR-Cytochrome P450s; alcoholic liver disease; mechanism; nutritional agent



Citation: Xiao, T.; Guo, Z.; Fu, M.; Huang, J.; Wang, X.; Zhao, Y.; Tao, L.; Shen, X. Amelioration of Alcoholic Liver Disease by Activating PXR-Cytochrome P450s Axis with Blackberry Extract. *Separations* **2022**, *9*, 321. <https://doi.org/10.3390/separations9100321>

Academic Editors: Jun Dang, Tengfei Ji and Xinxin Zhang

Received: 20 September 2022

Accepted: 17 October 2022

Published: 21 October 2022

Publisher's Note: MDPI stays neutral with regard to jurisdictional claims in published maps and institutional affiliations.



Copyright: © 2022 by the authors. Licensee MDPI, Basel, Switzerland. This article is an open access article distributed under the terms and conditions of the Creative Commons Attribution (CC BY) license (<https://creativecommons.org/licenses/by/4.0/>).

1. Introduction

Alcohol is regarded as a primary carcinogen by the international agency for research on cancer (IARC). According to the reports, more than 740,000 new cancer cases are associated with alcohol consumption in 2020, and it is critical to heightening public health intervention, which is crucial to mitigate the negative effect of alcohol [1].

The liver is the major organ of heterologous metabolism, and a multitude of toxic chemicals, and drugs could give rise to liver damage [2]. Alcoholic liver disease (ALD) is the main cause of the incidence rate and mortality of liver diseases. It results in fatty degeneration, hepatitis, progressive fibrosis, cirrhosis, liver cancer, and psychiatric illnesses [3,4].

Alcohol abuse and alcoholism have triggered a worldwide public health issue worldwide, and the burden of ALD accounts for 33% of all chronic liver diseases [5]. Many factors, such as nutrition, gene, heredity, and environment, are involved in the process of ALD degenerating into other serious diseases [6]. The forms of treatments, including nutritional therapy, drug therapy, psychotherapy, and liver transplantation depend on the different stages of liver disease. Abstinence is effective and essential to prevent ALD [7]. Corticosteroids have been used for the treatment of alcohol-associated hepatitis, which is the most extensive manifestation of ALD, for many decades [8]. The condition of macronutrient and micronutrient malnutrition is widespread in patients with ALD. Thus, the intake of supplemental protein and energy and some micronutrients is used as nutritional therapy [9]. Some anti-inflammatory agents and attractive targets have been studied in ALD therapies because of inflammation in liver injury associated with alcohol use [10]. Therapies for stimulating liver regeneration and a few agents with antioxidant properties have been considered as alternative options [3,11]. Unfortunately, these therapies for ALD have limited applicability and efficacy.

Pregnane X receptor (PXR), a member of metabolic NRs, plays a vital role in xenobiotic and endobiotic metabolism in mammals [12]. It is highly expressed in the liver and gastrointestinal tract. PXR could be activated by various ingredients, such as derivatives, pregnane steroids, and some herbal extracts. The ligand of PXR in active state is combined with retinoid X receptor alpha (RXR α) to form a heterodimer, which controls the transcription of various proteins encoding detoxification, such as phase I enzymes cytochrome P450, phase II enzymes sulfotransferases, glutathione transferases, and the transporters of metabolite elimination [13]. However, the physiological and pathophysiological roles of PXR on ALD remain unknown.

Berries have positive effects originating from their health-promoting benefits [14]. The World Health Organization (WHO) declares the natural anthocyanins from berries as excellent antioxidants. Blackberry (*Rubus fruticosus* Pollich), belonging to the family Rosaceae, is listed as a third-generation fruit and praised as the “black diamond” and “fruit of life” [15,16]. Moreover, it is one of the earliest fruits used for medicinal purposes due to its various nutritional ingredients. Blackberry is also a great source of multifarious active phytochemical constituents, especially anthocyanins and polyphenols, which have potential health benefits, such as anticancer, antioxidant, anti-inflammatory, antianxiety, antibacterial, hypoglycemic, hypolipidemic, liver protection, neuroprotection, and vascular protection [17–19]. The fruit of blackberry could be processed into foods, juice, wine, and syrup. Blackberry anthocyanins have been reported to impose obvious inhibitory effects on hepatic steatosis induced by oleic acid [20].

The activity of anthocyanins from black raspberry (*Rubus occidentalis* L.) against ALD has been studied by the authors in vivo and in vitro [21]. However, the ameliorative effect of blackberry, which is a different plant species with different chemical constituents, on ALD has never been reported. In the present study, the PXR-Cytochrome P450s axis was activated for ameliorating ALD with blackberry extract (BBE). Furthermore, the network pharmacology of cyanidin-3-O-glucoside was analyzed by molecular docking and networking. This study was the first to investigate BBE in terms of preventing ALD in vivo and in vitro.

2. Materials and Methods

2.1. Materials and Reagents

Blackberry was purchased from Youguowei organic blackberry and blueberry planting base, Nanjing, China. The voucher specimens (No. 202006) have been displayed in the herbarium of Guizhou Medical University. Cyanidin-3-O-glucoside, gallic acid, and catechin (the purity all higher than 95%) were purchased from Chengdu Purifa Technology Development Co., Ltd., Chengdu, China. The 2,2-diphenyl-1-picrylhydrazyl (DPPH), 2,2'-azino-bis (3-ethyl- benzothiazoline-6-sulfonic acid) (ABTS), 2,4,6-tris(2-pyridyl)-s-triazine (TPTZ), and Folin-Ciocalteu reagent were purchased from Sigma-Aldrich (St. Louis, MO,

USA). Ascorbic acid (V_C) was purchased from Sinopharm Chemical Reagent Co., Ltd., Shanghai, China. Fetal bovine serum, Dulbecco's Modified Eagle's medium (DMEM), and penicillin-streptomycin were purchased from Thermo Fisher Scientific Co., Ltd. (St. Wyman, Grand Island, MA, USA). MTT (3-(4,5-Dimethylthiazol-2-yl)-2,5-diphenyltetrazolium bromide) reagent was acquired from Guangzhou Solarbio Life Sciences Co., Ltd., Guangzhou, China. An Annexin V-FITC Kit (Cat. No.: 40302ES60) was purchased from Shanghai Yisheng Biotechnology Co., Ltd., Shanghai, China. JC-1 (Cat. No.: C2005) and a DCFH-DA (Cat. No.: S0033S) Kit were purchased from Beyotime Biotechnology Co., Ltd., Shanghai, China. Glyceraldehyde-3-phosphate dehydrogenase antibody (GAPDH, Cat. No.: 56t2759), nuclear factor-kappa b antibody (NF- κ B, Cat. No.: BF8005), transforming growth factor- β antibody (TGF- β , Cat. No.: AF1027), interleukin-6 antibody (IL-6, Cat. No.: DF6087), constitutive androstane receptor antibody (CAR, Cat. No.: DF6725) were purchased from Affinity Biosciences (USA), Shanghai, China, and pregnane x receptor antibody (PXR, Cat. No.: 118336, Abcame Biosciences (UK), Shanghai, China, Anti-alpha smooth muscle actin antibody (α -SMA, Cat. No.: ab7817) from Abcam Biosciences (UK), Shanghai, China. Ethanol and HCl of analytical purity were purchased from Merck Chemical Technology (Shanghai) Co., Ltd., Shanghai, China.

2.2. Preparation of the Blackberry Extract

We refer to our previous research and the stability of anthocyanins under acidic conditions [22]. Blackberry fresh fruits were washed and vacuum freeze-dried, and then powdered. A total of 300 g powder was extracted by ultrasonic with ethanol-water (75:25, *v/v*, containing 0.1% HCl) at 35 °C 3 times, each time lasting for 1 h to obtain 70 g of blackberry extract (BBE), which was rich in crude anthocyanins, and then filtered with a Buchner funnel. BBE was obtained after the solvents were removed under vacuum using a rotary evaporation device, and the BBEs were stored at -20 °C before use. All processes are dark operations with black film and tin foil wrapping and stored away from light.

2.3. Polyphenol, Flavonoids, and Anthocyanin Contents

The experiments were implemented according to our previous research [22]. The Folin-cioaltea method was used to detect the total phenolic content (TPC) of BBE, which was expressed as mg GAE/g DW according to the gallic acid calibration curve. The content of total flavonoids (TFC) in the BBE was determined by colorimetry, and the results were expressed as the average of milligrams catechin equivalents (CE)/g dry weight (DW). The anthocyanin content (TMA) was determined by the pH differential method [23], and the results were calculated as mg of cyanidin-3-O-glucoside equivalents/g dry weight (DW).

2.4. Antioxidant Activities

We refer to the method reported previously [22]. The antioxidant capacity of BBE was conducted with DPPH and ABTS radical scavenging assays and ferric reducing antioxidant power (FRAP) assays. Vitamin C was the antioxidant standard.

2.5. Animals and Treatment

2.5.1. Animals

Male Kunming mice weighing 18.0–22.0 g were purchased from the experimental animal center of Guizhou Medical University. The animals were subjected to a cycle of 12 h light/dark with conditions of 22 °C in an animal room free of specific pathogens with a humidity of 60% \pm 5%. They were allowed free access to water and food. All animal operating procedures obey the regulations on animal experiments issued by the National Science and Technology Commission of the People's Republic of China and the guidelines for the care and use of laboratory animals issued by the National Institutes of Health (Experimental facility certification No.: SYXK (Guizhou) 2018-0001).

2.5.2. Experimental Design

The mice were adaptively fed for one week and randomly assigned to 10 groups with 10 mice per group. During the experiment, records of the food and water intake of mice once a day were processed. In acute and subacute ALD mice, these groups included a control group, a model group, and three treatment groups (25, 50, and 100 mg BBE/kg BW; suspension was prepared with 0.5% carboxymethyl cellulose CMC). The experiment lasted for one month, carried out as reported previously [21] (Figure 1). The control group was intragastrically administered an equal volume of saline during the experiment. In the acute experiment, the low, medium, and high dose groups were intragastrically administered with corresponding doses of BBE once, and the model group was administered with an equal volume of saline. Four hours after the last administration, the model and treatment groups were given 50% ethanol by gavage (12 mL/kg BW). All groups fasted for 16 h, and the mice were anesthetized by an intraperitoneal injection of pentobarbital sodium 60 mg/kg BW.

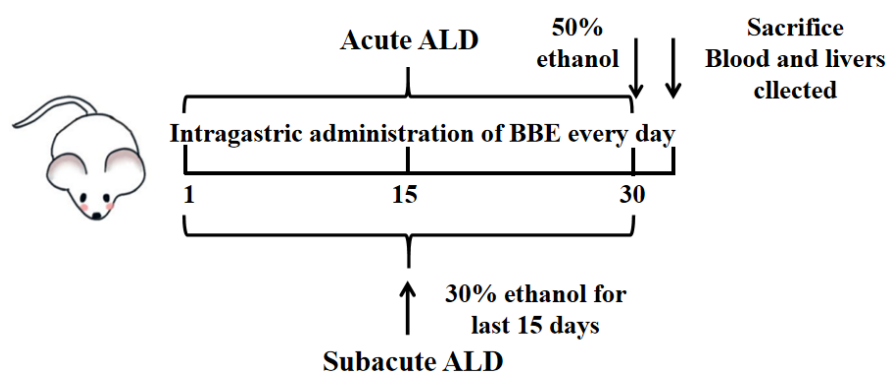


Figure 1. Experimental protocol for the establishment of ALD and the treatment schedule.

In the subacute experiment, the model group was given the same dose of saline for 15 days once a day, and the next with 30% ethanol (10 mL/kg BW) for 15 days. The low-, medium-, and high-dose groups were given BBE for 30 days and then treated with 30% ethanol once a day for the last 15 days. The interval between the two administrations was 4 h. Then, all groups fasted for 4 h, and all mice were anesthetized with pentobarbital sodium.

2.5.3. Measurement of Related Indices

The percentage of liver weight/body weight was used to calculate liver indexes. Blood was collected from the retroorbital venous plexus and the levels of aspartate aminotransferase (AST), Alanine aminotransferase (ALT), superoxide dismutase (SOD), and malondialdehyde (MDA) were measured. After coagulation, AST, ALT, SOD, and MDA in serum were detected by an automatic biochemical analyzer (Chemray 800, Shenzhen redu Life Technology, Shenzhen, China)

2.5.4. Histopathological Observation

All mouse livers were fixed in 4% paraformaldehyde for 48 h with paraffin-embedded tissues and cut into sections 5–6 μm thick. They were then placed on microscope slides for H&E staining and Sirius red staining and then observed under a microscope (Mshot MF53, Mingmei Photoelectric Technology Co., Ltd., Guangzhou, China).

In addition, oil red O staining with a 10 μm frozen section of liver tissue was applied to evaluate steatosis under a microscope.

2.5.5. Network Pharmacological Analysis of Cyanidin-3-O-glucoside

We searched the SMILES number of cyanidin-3-O-glucoside in the PubChem database (the main component of BBE) and then entered the Swiss Target Prediction Database

(<http://www.swisstargetprediction.ch/>) (accessed on 1 September 2020). The species was defined as “Homo sapiens”, and the targets related to cyanidin-3-*O*-glucoside were acquired. The keyword “ALD” was used in the GeneCards Database (<https://www.genecards.org/>) (accessed on 15 September 2020), and the condition was “score > 20”; the targets related to ALD were selected. Then, the screened component targets and disease targets of cyanidin-3-*O*-glucoside and ALD were located to obtain the cross targets with Venn diagrams (<http://bioinformatics.psb.ugent.be/webtools/Venn/>) (accessed on 30 September 2020).

2.5.6. Establishment of PPI Network

The cross-targets of active components and disease were inputted into the STRING Database (<https://string-db.org/>) (accessed on 5 October 2020). The species was “H. sapiens”, and the selected condition was the comprehensive score of protein interaction > 0.4. Then, the relationship between the target interaction network and PPI was established. Then, the Cytoscape 3.7.2 software was used for network data analysis with the TSV format exported from the network.

2.5.7. Analysis of Target Pathways

R × 64 (4.0.2) was used for the analysis of the intersection targets for the enrichment analysis of the GO and KEGG pathways. The top 20 channels were collected, and a visual analysis of the histograms was displayed.

2.5.8. Construction of Regulatory Network for Cyanidin-3-*O*-glucoside-Targets-Pathways-Disease

From the enrichment analysis of the KEGG results, the construction of 18 low *p*-value target pathways related to ALD was carried out, and the Cytoscape 3.7.2 software was processed to construct the “components-target pathway-disease” network with the common targeting. In the established network, the putative targets of cyanidin-3-*O*-glucoside on ALD were marked green, while the pathways related to ALD were marked red. The interactions between cyanidin-3-*O*-glucoside, targets, pathways, and disease were represented by black edges.

2.5.9. Analysis of Gene Ontology and KEGG

The molecular function (MF), biological process (BP), and cellular component (CC) were collected from the Gene Ontology (GO) Database (<http://geneontology.org/>) (accessed on 25 October 2020), which can be used to predict the biological mechanisms analysis of high-throughput genomic or transcriptome data. The compound was cyanidin-3-*O*-glucoside and targeted ALD. The function and biological correlation of candidate targets can be selected in the KEGG database (<https://www.kegg.jp/>) (accessed on 25 October 2020) [24]. In the study, the analysis of the GO and KEGG pathways was carried out with the “ClusterProfiler” package in R. In these enrichment analysis results, the name of the pathway was located on the Y-axis, and the X-axis was the enrichment factor. The bubble size represented the number of genes belonging to this pathway in the target genes, and the bubble color was the degree of enrichment, i.e., the value of *p*.adjust. The threshold was set to *p*-value < 0.01.

2.5.10. In Silico Molecular Docking Study

The top one of the KEGG pathways in the drug-target network was selected for molecular docking. In order to evaluate the efficacy of the main anthocyanins (cyanidin-3-*O*-glucoside) in BBE as inhibitors of PXR [25], Cyt P450 1B1, Bcl-2, Caspase 9, and an activator of Cytochrome c, the analysis of molecular docking was processed to predict the ligand within the restriction of receptor binding sites. The crystal structures of PXR, Cyt P450 1B1, Bcl-2, Caspase 9, and Cytochrome c were downloaded with IDs 1NRL, 3PM0, IDs, 4LVT, 4RHW, 2BC5 from PDB. ChemBioDraw (PerkinElmer) and AutoDock Tools

(ADT, version: 1.5.6) were used for the docking process, and the structure exhibition was displayed by Discovery Studio 2016 Client. Genetic Algorithm was used for Blind docking, and the conformations of the most favorable binding energy were used to investigate the resultant complex structures.

2.5.11. qRT-PCR Analysis

The total RNA of liver tissue was extracted and isolated with a total RNA kit (Wuhan Servicebio Technology Co., Ltd., Wuhan, China) for qRT-PCR under the guidance of the instructions, and then the cDNA was synthesized. RT-PCR amplification scheme was as follows: initial denaturation at 95 °C for 10 min, denaturation at 95 °C for 15 s, annealing at 60 °C for 30 s, melting curve at 65 °C to 95 °C, temperature rise 0.3 °C every 15 s, and cycle 40 times. The transcription level was related to the *GAPDH* mRNA level, and the transcription levels were calculated by the $2^{-\Delta\Delta CT}$ method. All the above primers were synthesized by Wuhan Servicebio Technology Co., Ltd., (Wuhan, China). The primers are listed in Table 1.

Table 1. Quantitative real-time PCR primers.

Gene	Forward (5'-3')	Reverse (5'-3')
<i>PXR</i>	AGACGGCAGCATCTGGAACACTAC	GTTTCTGGAAGCCACCATTAGG
<i>CAR</i>	CCACAGGCTATCATTCCACG	CCTTCCAGCAAACGGACAGAT
<i>CYP3A25</i>	GGAGGCCTGAACTGCTAAAG	GTAGTTGAAAATGGTGCCAAGTAAC
<i>CYP3A11</i>	GGTGCTCCTAGCAATCAGCTT	AAGGAGAGGCGTTTGACCATC
<i>CYP2B10</i>	TCTGCCCTTCTCAACAGGAAAG	AAGGAGAGGCGTTTGACCATC
<i>GAPDH</i>	TTGGAGCCCTGGAGATTTGGA	TGAGGTCAATGAAGGGGTCGT

2.6. Potential Mechanisms of BBE against HepG2 Cells

2.6.1. Cell Viability Assay

The cytotoxicity of HepG2 cells induced by 200 mM ethanol was measured with an MTT assay. Cells (5000 cells/well) were inoculated into 96-well plates and cultured overnight. Then, the cells were treated with a mixture of 200 mM ethanol and different concentrations of BBE (150, 250, and 450 µg/mL, dissolved in PBS) for 24 h. After the treatments, formazan crystals were then formed after 0.5 mg/mL MTT was added to each well and cultured for 4 h. After removing the supernatant, 150 µL DMSO was added to dissolve the crystals. The absorbance of formazan crystals formed was quantified at 490 nm using a microplate reader (Bio-Rad iMARK, Berkeley, CA, USA). The data were calculated as a percentage of survival compared with untreated control cells.

2.6.2. Detection of Apoptosis by Flow Cytometry in HepG2 Cells

Referring to the manufacturer’s instructions (ACEA Bioscience, Inc., Hangzhou, China), the Annexin V-FITC apoptosis kit was used to determine the apoptotic effect induced by the mixture of 200 mM ethanol and different concentrations of BBE. In short, HepG2 cells were spread evenly on a six-well plate (2×10^5 /well) and incubated for 24 h. After the treatment of 200 mM ethanol and different concentrations of BBE for 24 h, the cells were collected by centrifugation and washed with PBS. Thereafter, 100 µL binding buffer was added to resuspend cells and Annexin V-FITC and propidium iodide were used to stain for 15 min in the dark at room temperature. At last, the cells were evaluated by flow cytometry after staining within 1 h, and the data were analyzed using NovoExpress software (version 1.2.5) (ACEA Bioscience, Inc., Hangzhou, China).

2.6.3. Measurement of Mitochondrial Membrane Potential in HepG2 Cells

JC-1 kit was used to measure the loss of mitochondrial membrane potential by fluorescent probe under the guidance of instructions. The cultured cells were incubated with a 2.0 mg/mL JC-1 fluorescent probe for 30 min at 37 °C. After washing with ice-cold PBS, HepG2 cells were observed on a Leica DM4B inverted microscope (100× magnification).

The loss of mitochondrial membrane potential drives the formation of red fluorescing JC-1 dimers.

2.6.4. Detection of ROS Levels in HepG2 Cells

HepG2 cells were treated with 200 mM ethanol, and DCFH-DA fluorescent probe was used to detect intracellular reactive oxygen species (ROS). In brief, HepG2 cells were diluted into approximately 2×10^5 cells/well on 6-well plates (JET BIOFIL, Guangzhou, China) in DMEM medium (Gibco, Grand Island, NY, USA) using a DCFH-DA fluorescent probe for 10 min, and luminescence was detected by flow cytometry at the excitation wavelength of 488 nm and emission wavelength of 525 nm, and the data were analyzed using NovoExpress software.

2.7. Western Blotting

After treatment, the mice livers or cells were obtained, and the total proteins were collected from the tissue or cells using RIPA lysis buffer, and a BCA assay was used to measure the concentration. Briefly, 10% SDS-PAGE was used to separate equal amounts of proteins, then proteins were transferred to polyvinylidene fluoride membranes. Additionally, membranes were incubated with NF- κ B (1:2000), TGF- β (1:2000), PXR (1:3000), IL-6 (1:1000), CAR (1:1000), and α -SMA (1:2000) antibodies and Bax (1:2000) antibodies overnight at 4 °C. Membranes and the appropriate secondary antibodies were incubated together for 1 h at room temperature. Then, ECL reagents (Beyotime Institute of Biotechnology, Shanghai, China) were used to display positive bands with the ChemiDoc MP Imaging System (Bio-Rad, Hercules, CA, USA). The protein blot intensities were quantified using Image J Software (1.48 v) and normalized to the housekeeping protein (GAPDH) levels.

2.8. Data and Statistical Analysis

All data were repeated three times, and the values are expressed as mean \pm SD. One-way analysis of variance (ANOVA) was used to test differences between groups, and LSD was used for average separation ($p \leq 0.05$) using the GraphPad Prism program (Version 6.01) for statistical analysis.

3. Results

3.1. The Contents of Polyphenols, Flavonoids, and Anthocyanins

In BBE, the total polyphenols and flavonoids of blackberry were 5.70 ± 1.34 and 105.70 ± 12.11 mg/g DW, respectively (Table 2). Polyphenols and flavonols, which are almost completely glycosylated, are rich in berries [26]. For instance, the highest content of ellagic acid in blackberry of the Boysen variety was 13.67% [27]. The total monomeric anthocyanin content of blackberry was 24.50 ± 3.49 mg/g DW. Cyanidin, the main anthocyanin in blackberry fruits, especially cyanidin-3-O-glucoside, accounts for more than 80% of total anthocyanins [25].

Table 2. The total phenolic contents, total flavonoid, total monomeric anthocyanin, and the antioxidant activities of DPPH, ABTS, and FRAP assays of blackberry.

Species	TP ^a	TF ^b	TMA ^c	DPPH ^d	ABTS ^d	FRAP ^e
Blackberry	5.70 ± 1.34	105.70 ± 12.11	24.50 ± 3.49	22.08 ± 7.13	51.69 ± 7.84	2.93
Vc				4.76 ± 1.15	36.23 ± 5.78	1

Values with the different superscript in the same column indicate significant statistical differences ($p < 0.05$); n = 3.

^a The total phenolic (TP) content of species is expressed as mg gallic acid equivalents (GAE)/g dry weight (DW).

^b The total flavonoid (TF) content of species is expressed as mg catechin equivalents (CE)/g dry weight (DW).

^c The total monomeric anthocyanin (TMA) is expressed as mg cyanidin-3-O-glucoside equivalents/g dry weight (DW). ^d The DPPH and ABTS activities are expressed as EC₅₀ and IC₅₀ in μ g/mL for extracts. ^e In FRAP activities, the value "1" of Vc was defined as the quantity of Vc generating 100 μ M Fe²⁺, and the value of species is expressed as the times of the ability of Vc.

3.2. Antioxidant Activities

The results of the DPPH assay confirmed that the radical scavenging activities of BBE were lower than that of the positive control (V_C, 4.76 ± 1.15 µg/mL), with EC₅₀ of 22.08 ± 7.13 µg/mL. Similar conclusions were found in the ABTS assay with an EC₅₀ of 51.69 ± 7.84 µg/mL of BBE, which was weaker than the V_C (36.23 ± 5.78 µg/mL) for free radical scavenging capacity. The results indicated that BBE has good free radical scavenging ability. In the FRAP assay, the FRAP value was expressed as a µM FeSO₄/µM sample under the same absorbance. The FRAP value of BBE was 2.93, indicating that it is a powerful ferric-reducing antioxidant compared with vitamin C. The results suggested that BBE possesses excellent electron-transfer capacity and total antioxidant activity (Table 2) [22,28].

3.3. Measurement of Related Indices

The effects of BBE on growth performance and liver indices were displayed in Table 2. The liver weight and index of the BBE-treated groups decreased with no significant difference compared with those of the model group. Meanwhile, no difference was observed in the liver weight among the low-, medium-, and high-dose BBE groups in the acute and subacute ALD experiments.

In the acute and subacute ALD experiments, the levels of ALT, AST, and MDA in the model groups increased, whereas the SOD level decreased. In the treatment groups (low-, medium-, and high-dose groups), these markers shifted distinctly to normal levels in a dose-dependent manner. The results (Table 3) indicated that administering BBE enormously suppressed liver injury, lessened the release of these markers into blood, and promoted the antioxidant capacity of liver tissues. In the subacute ALD experiments, the treatment groups showed extensive enhancement compared to the model group (*p* < 0.001). The reason may be related to the inhibitory effects of anthocyanins with strong antioxidant activity in oxidative stress, which resulted in ALD [29]. This study is the first investigation of blackberry on the inhibitory effect on ALD in vivo.

Table 3. Effect of BBE on the activity of biochemical parameters.

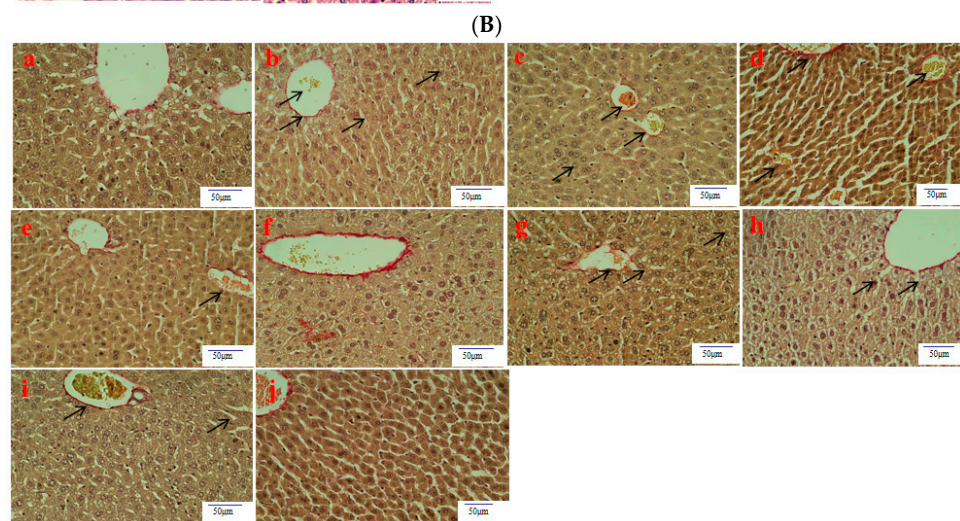
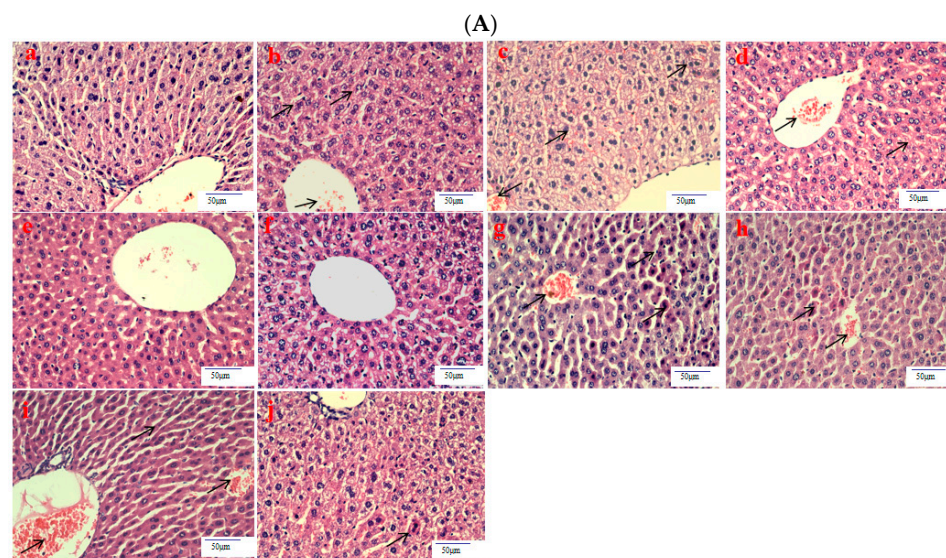
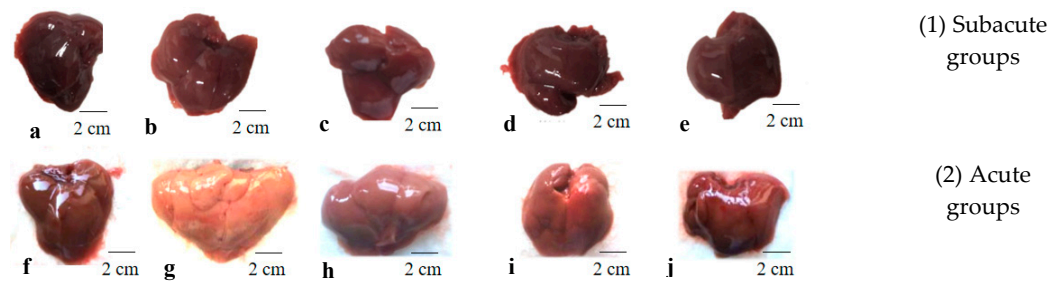
Treatment Group	Final Weight (g)	Liver Index (%)	AST (U/L)	ALT (U/L)	SOD (U/mL)	MDA (U/mL)
(a) Subacute ALD mice						
Control	41.45 ± 2.78	4.23 ± 0.24	135.60 ± 8.75	55.07 ± 7.03	260.13 ± 17.52	5.76 ± 0.24
Model	34.48 ± 3.45	3.76 ± 0.31	189.92 ± 15.87 ***	94.08 ± 1.55 ***	177.88 ± 3.24 ***	11.37 ± 0.14
Low-dose BBE	36.69 ± 4.05	3.81 ± 0.55	169.60 ± 11.35 ###	82.01 ± 1.09 ###	191.01 ± 2.89 ###	8.79 ± 0.24 ###
Medium-dose BBE	35.87 ± 3.61	3.71 ± 0.39	163.73 ± 10.24 ###	72.28 ± 2.23 ###	229.02 ± 6.96 ###	8.19 ± 0.65 ###
High-dose BBE	36.12 ± 3.34	3.69 ± 0.25	151.18 ± 5.27 ###	61.57 ± 3.97 ###	235.07 ± 3.15 ###	8.03 ± 0.42 ###
(b) Acute ALD mice						
Control	40.90 ± 0.45	3.29 ± 0.30	121.14 ± 9.95	44.71 ± 7.13	306.80 ± 17.14	6.37 ± 0.42
Model	41.00 ± 0.31	4.30 ± 0.21	210.14 ± 22.60	72.65 ± 0.55	231.62 ± 4.29	8.94 ± 0.21
Low-dose BBE	41.31 ± 0.62	4.04 ± 0.57	176.69 ± 14.77	70.82 ± 1.19	245.44 ± 3.58	8.49 ± 0.08
Medium-dose BBE	41.58 ± 0.45	3.33 ± 0.22	158.99 ± 10.16	60.01 ± 1.23	253.22 ± 7.68	7.28 ± 0.16
High-dose BBE	41.69 ± 0.56	3.10 ± 1.27	151.37 ± 3.76	53.94 ± 4.97	266.19 ± 2.55	7.12 ± 0.21

Values are the mean ± standard deviation of 10 determinations. Compared with control: ***, *p* < 0.001. Compared with model: ###, *p* < 0.001.

3.4. Histopathological Observation

Histological evaluation is applied to assess the severity of ALD. In this study, it was used to estimate the amelioration of BBE on hepatic steatosis, hepatic fibrosis, and liver pathological changes on the basis of liver sections. Representative micrographs of the liver histology were elucidated in Figure 2. In the acute or subacute ALD experiments, the control groups exhibited normality in appearance, color, and liver status (Figure 2A). On the contrary, the livers of the model groups were pale, hard, large, and rough. The pathological state of the liver treated with BBE was modified in a dose-dependent manner, coinciding with the results of the pathological sections. In the H&E staining (Figure 2B), the subjects in the acute or subacute ALD experiments exhibited a large amount of fat accumulation and a process into steatohepatitis and fibrosis, which were characterized

by hepatocyte expansion, scattered lobular inflammatory cell infiltration, inflammatory lesions, and some severe cellular fibrosis. After Sirius red staining was applied in the model group (Figure 2C), collagen fibers extended outward along the vascular wall of the portal area, and the amount of product was significantly higher than that in the control group. Obvious changes in the morphology of hepatocytes, such as cell cavities, uneven arrangement, and cell shrinkage, were observed. The accumulation of fat, steatohepatitis, and fibrosis were eased when the animals were administered BBE. In addition, a large area of fat deposition and a large, dark halo of fat droplets were detected in the model group after oil red O staining (Figure 2D). These results indicated that BBE relieved hepatic steatosis, necroinflammation, and hepatic fibrosis.



(C)
Figure 2. Cont.

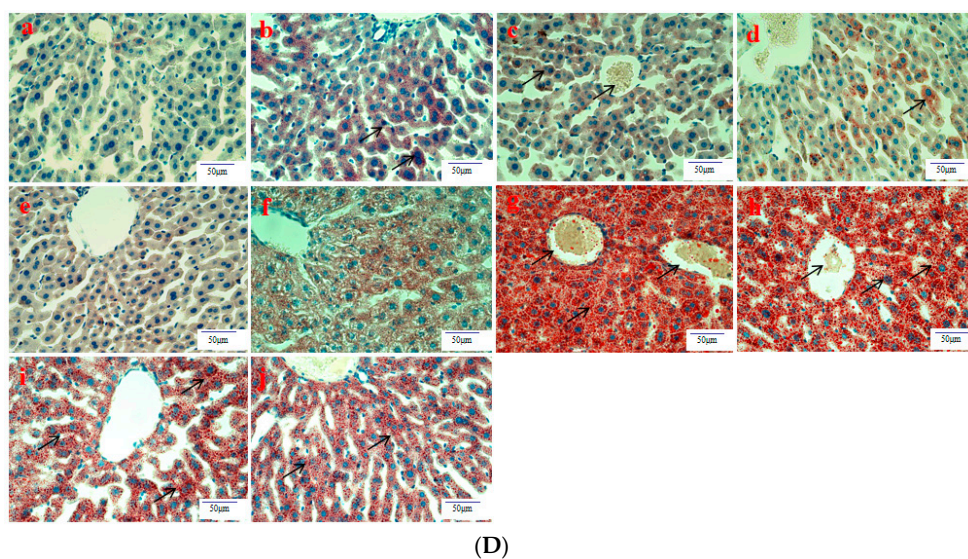


Figure 2. The histopathological observation of BBE on subacute and acute alcohol-induced liver damage (liver appearance, (A); analysis of BBE with H&E staining ((B), $\times 400$), Sirius red staining ((C), $\times 400$), and oil red O staining ((D), $\times 400$) ((a), subacute control group; (b), subacute model group; (c), subacute low-dose BBE group; (d), subacute medium-dose BBE group; (e), subacute high-dose BBE group; (f), acute control group; (g), acute model group; (h), acute low-dose BBE group; (i), acute medium-dose BBE group; (j), acute high-dose BBE group)).

3.5. Network Pharmacological Analysis of Cyanidin-3-O-glucoside

The SMILES number of cyanidin-3-O-glucoside retrieved on the PubChem database was C1=CC(=C(C=C1C2=[O+]C3=CC(=CC(=C3C=C2OC4C(C(C(C(O4)CO)O)O)O)O)O)O. A total of 100 related targets of cyanidin-3-O-glucoside were searched on the Swiss Target Prediction database (Figure S1A). A total of 5389 ALD-related targets were screened on the GeneCards database to reveal a Venn diagram (Figure S1B). These two kinds of targets were mapped to each other to collect 82 shared targets (Table S1).

3.6. Establishment of PPI Network

The shared targets between cyanidin-3-O-glucoside and ALD were inputted into the STRING database, and the protein interaction network was conducted on Cytoscape 3.7.2 (Figure S2). A total of 82 nodes and 112 edges were surveyed in the network. The average degree of nodes and the local clustering coefficient were 10.6 and 0.519, respectively. Refined with degree value, the degrees of AKT1, TNF, SRC, EGFR, PTGS2, and PIK3R were greater than the average node degree.

3.7. Analysis of Target Pathways

As a key technology in systems biology, network pharmacology attaches great importance to the molecular mechanism of complex diseases [30]. As shown in Figure S3A–C, the top five PPI network targets involved in the metabolic process were the response to oxidative stress, the cellular response to chemical stress, the cellular response to oxidative stress, peptidyl-tyrosine phosphorylation, and peptidyl-tyrosine modification. The analysis of CC demonstrated that these targets are related to the membrane raft, membrane microdomain, cell projection membrane, membrane region, and apical part of the cell, which are ranked as the top five. According to the analysis of MF, the top five targets were connected with protein serine/threonine kinase activity, protein tyrosine kinase activity, transmembrane receptor protein tyrosine kinase activity, transmembrane receptor protein kinase activity, and lyase activity.

As shown in Figure S4, enrichment analysis of the KEGG pathway showed that these targets involved signal pathways including EGFR tyrosine kinase inhibitor resistance, proteoglycans in cancer, nitrogen metabolism, endocrine resistance, and PI3K-Akt, which were in the top five. These results certified that the targets of cyanidin-3-*O*-glucoside were distributed in different metabolic pathways. The mechanism of ALD treatment is possible “multi-targets, and multi-pathways” mutual regulation.

3.8. Construction of Regulatory Network for Cyanidin-3-*O*-glucoside-Targets-Pathways-Disease

An interaction network was conducted on Cytoscape 3.7.2 to clarify the mechanism of cyanidin-3-*O*-glucoside on ALD. The pathway diagram of “component-target-pathway-disease” was shown in Figure S5. The network consisted of 224 nodes and 434 edges. Among the nodes, 82 nodes were green, indicating these targets were common, and 29 nodes were red, which suggested these were related to KEGG pathways. The pink and yellow nodes were cyanidin-3-*O*-glucoside and ALD, respectively. According to the degree of the pathway, the mechanisms involved were EGFR tyrosine kinase inhibitor resistance, proteoglycans in cancer, nitrogen metabolism, endocrine resistance, and the PI3K-Akt signaling pathway and other pathways. In this study, the PI3K-Akt signaling pathway was selected for mechanism verification.

3.9. In Silico Molecular Docking Study

As an important tool of computer-aided molecular design, molecular docking predicts biological experiments that were conducted by simulating the interaction between small molecules and biological macromolecules.

The binding energy and binding mode of cyanidin-3-*O*-glucoside with PXR, Cyt P450 1B1, Bcl-2, Caspase 9, and as Cytochrome c activator were shown in Table 4 and Figure 3. The lower the binding energy is, the easier it is to bind to proteins. Cyanidin-3-*O*-glucoside was transplanted compatibly into the binding domain of Cyt P450 1B1, Bcl-2, Caspase 9, and Cytochrome c, and binding energies were -8.7 , -8.2 , -7.3 , -7.2 , and -7.6 kcal/mol, respectively. Furthermore, cyanidin-3-*O*-glucoside bound to PXR easily and it was matched with the PXR-Cytochrome P450s axis appropriately.

Table 4. Molecular docking mode for Cyanidin-3-*O*-glucoside with PXR, Bcl-2, Caspase 9, and Cytochrome c.

Targets	Binding Free Energy (kcal/mol)	Numbers of Bonds
PXR	-8.7	10
Cyt P450 1B1	-8.2	14
Bcl-2	-7.3	6
Caspase 9	-7.2	5
Cytochrome c	-7.6	4

3.10. qRT-PCR Analysis

The mRNA level of liver tissues was detected by qRT-PCR to determine the expression of the PXR-Cytochrome P450s axis in ALD. In the acute and subacute experiments, PXR decreased significantly in the model groups ($p < 0.05$). It increased significantly in the low-dose BBE group of the acute model ($p < 0.001$), and the medium- and high-dose BBE groups ($p < 0.001$) of the subacute model (Figure 4A).

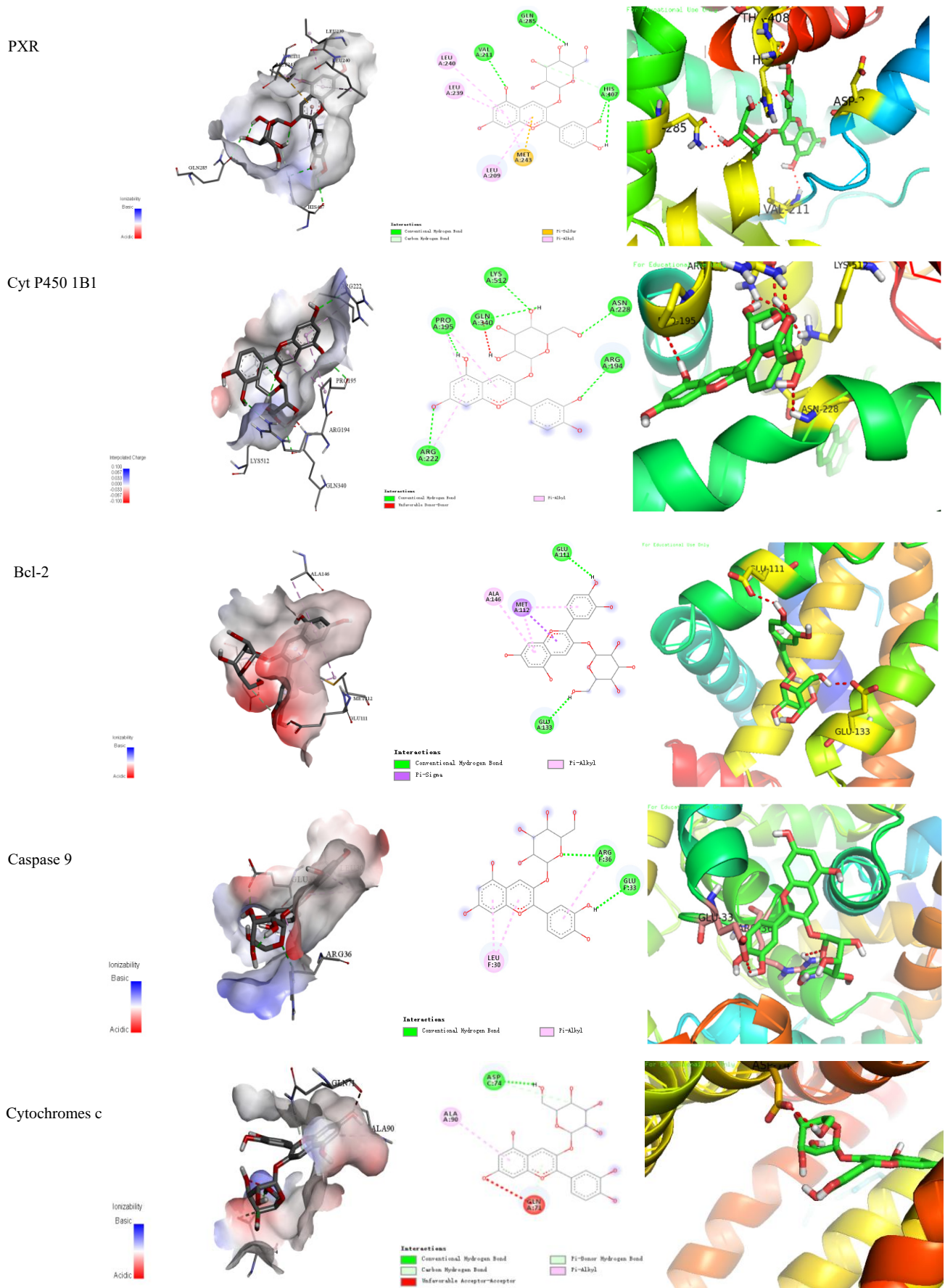


Figure 3. Cyanidin-3-O-glucoside-proteins docking combination.

The mRNA expression of *CAR* in the model group decreased in the acute ALD mice and increased in the low-, and medium-dose BBE groups. Meanwhile, no significant difference was found between the model group and the control group, and between the BBE groups and the model group. In the subacute ALD mice, *CAR* increased significantly ($p < 0.05$) in the high-dose BBE groups (Figure 4B).

Similarly, the mRNA expression of *CYP3A25* (Figure 4C), *CYP3A11* (Figure 4D), and *CYP2B10* (Figure 4E) were reduced in the model groups of acute and subacute experiments and increased in all BBE groups. A notable detail is that *CYP2B10* decreased significantly ($p < 0.01$) in the model group, and increased significantly ($p < 0.05$) in the high-dose BBE group of the acute experiment. Meanwhile, *CYP3A25*, *CYP3A11*, and *CYP2B10* enhanced significantly in the high-dose BBE group of the subacute experiment. The results indicated that the benefits of BBE in subacute ALD are superior to that in acute ALD.

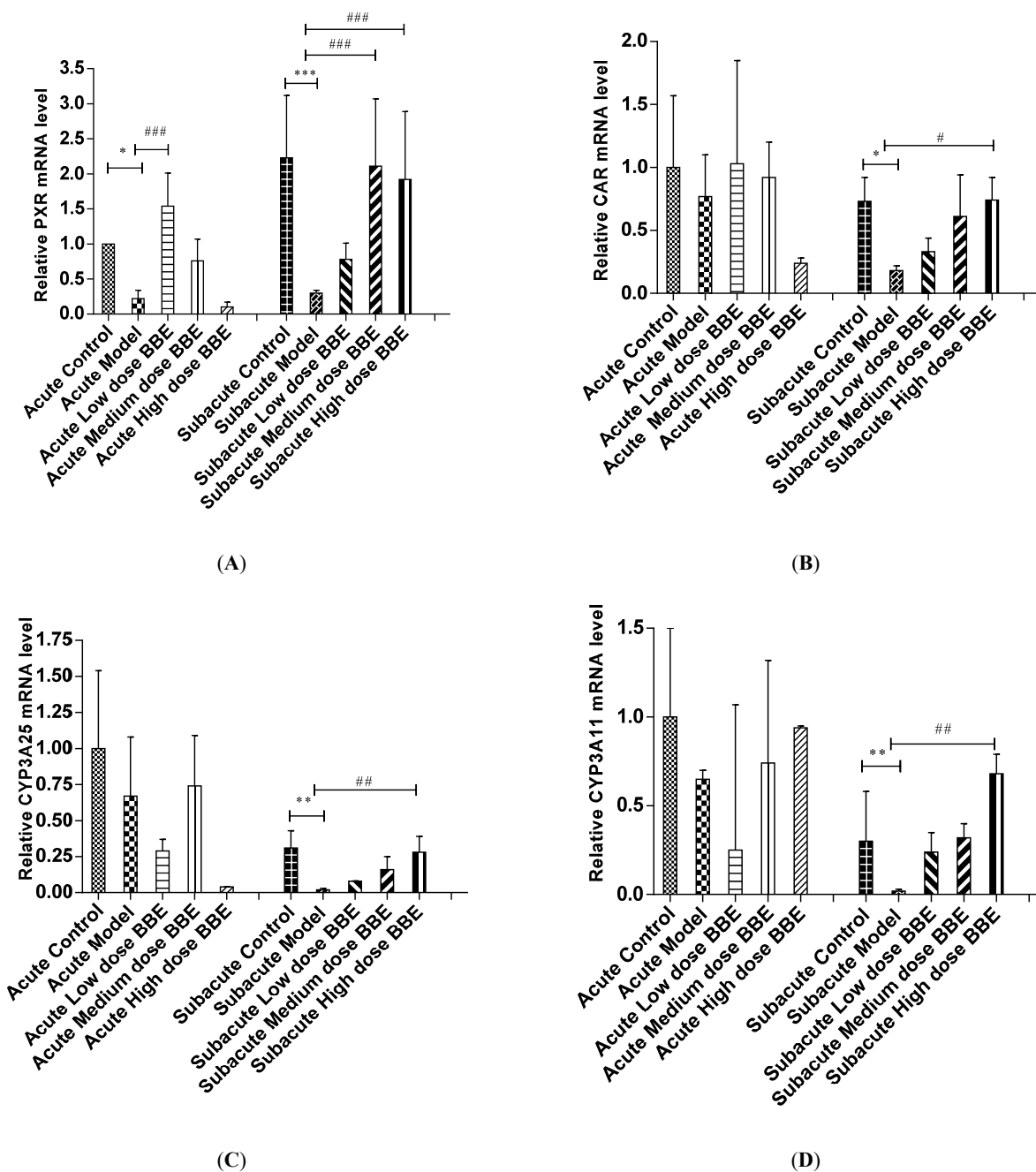
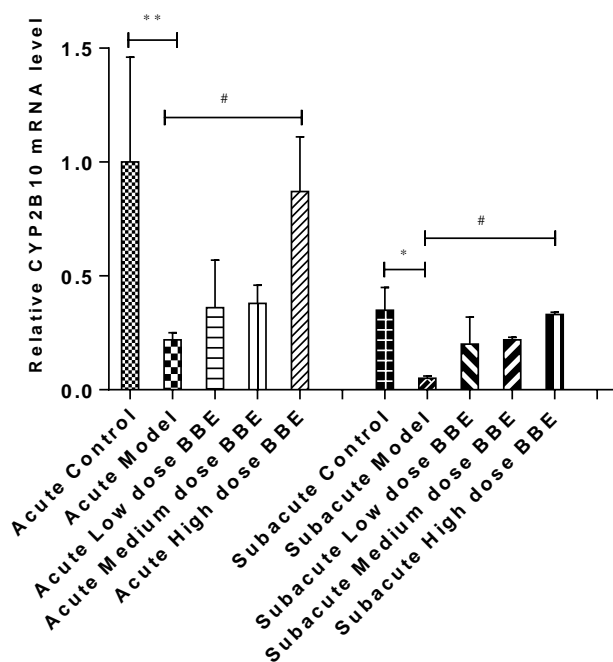


Figure 4. Cont.



(E)

Figure 4. The qRT-PCR analysis of the PXR-Cytochrome P450s axis in ALD (A–E). Values are the mean \pm standard deviation. Compared with control: *, $p < 0.05$; **, $p < 0.01$; ***, $p < 0.001$. Compared with model: #, $p < 0.05$; ##, $p < 0.01$; ###, $p < 0.001$.

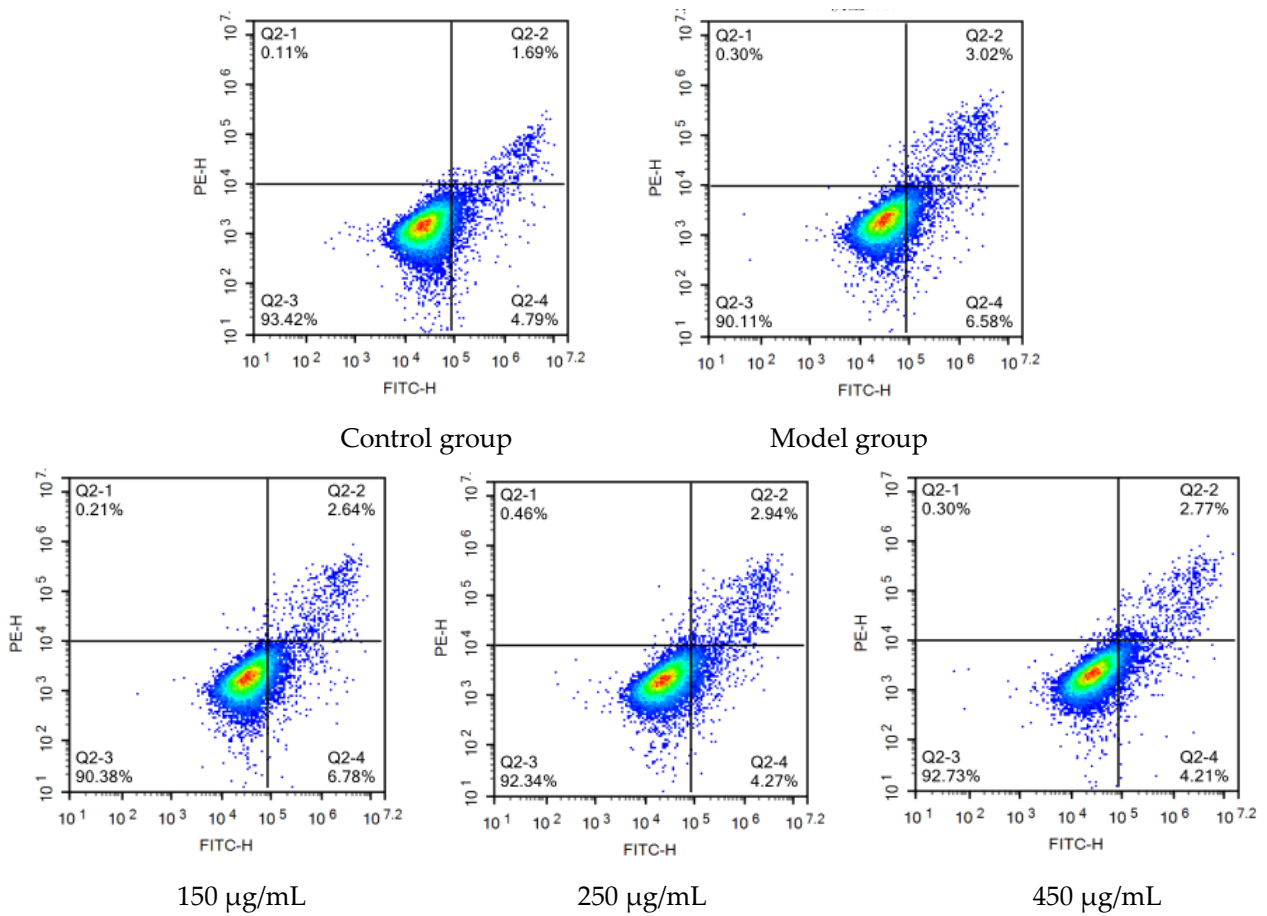
3.11. Detection of Apoptosis by Flow Cytometry in HepG2 Cells

The injury of HepG2 cells induced by 200 mM ethanol was used to simulate the effect of ALD in vitro and explore the effect of BBE on ALD. An Annexin V-FITC assay was carried out to determine the effects of BBE on the apoptosis of HepG2 cells.

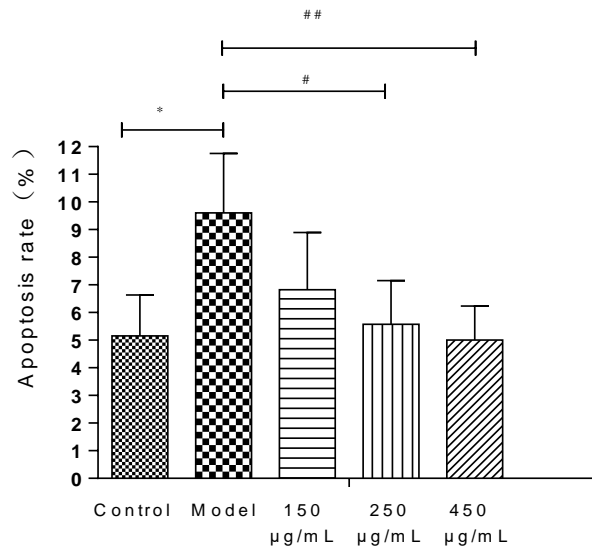
BBE upgraded the cell viability in a dose-dependent manner in HepG2 cells (Figure 5A,B). Late and early apoptotic cells appeared in Q2 and Q4, respectively. The results suggested that BBE (150, 250, and 450 $\mu\text{g}/\text{mL}$) ameliorated ethanol-induced apoptosis compared with the model group. The apoptotic rates of the control group, the model group, and the low-, medium-, and high-dose groups were $6.48 \pm 1.48\%$, $9.60 \pm 2.15\%$, and $9.42 \pm 2.07\%$, $7.21 \pm 1.58\%$, and $6.98 \pm 1.23\%$, respectively. The middle- ($p < 0.05$) and high-dose BBE groups ($p < 0.01$) showed a significant protective effect on the ethanol-induced apoptosis of HepG2 cells.

3.12. Measurement of Mitochondrial Membrane Potential in HepG2 Cells

Changes in the mitochondrial membrane potential of HepG2 cells were studied to examine whether the improvement of this event is consistent with the antiapoptotic effect of BBE. With the depolarization of the mitochondria, the cell fluorescence changed from red to green with the help of membrane-permeant JC-1 dye (Figure 6). The results revealed that the intensity of red fluorescence decreased in the model group, suggesting progressive depolarization in the mitochondria. The intensity of red fluorescence increased with the pretreatment of BBE and 200 mM ethanol. The results were consistent with those of the Annexin V-FITC analysis pretreated with BBE previously. Overall, these results indicated that BBE prevents mitochondrial membrane depolarization induced by ethanol, and anthocyanins, especially cyanidin-3-O-glucoside, may be the active components.



(A)



(B)

Figure 5. Annexin V-FITC Apoptosis Detection by Flow Cytometry in HepG2 cells (A,B). Values are the mean \pm standard deviation. Compared with control: *, $p < 0.05$. Compared with model: #, $p < 0.05$, ##, $p < 0.01$.

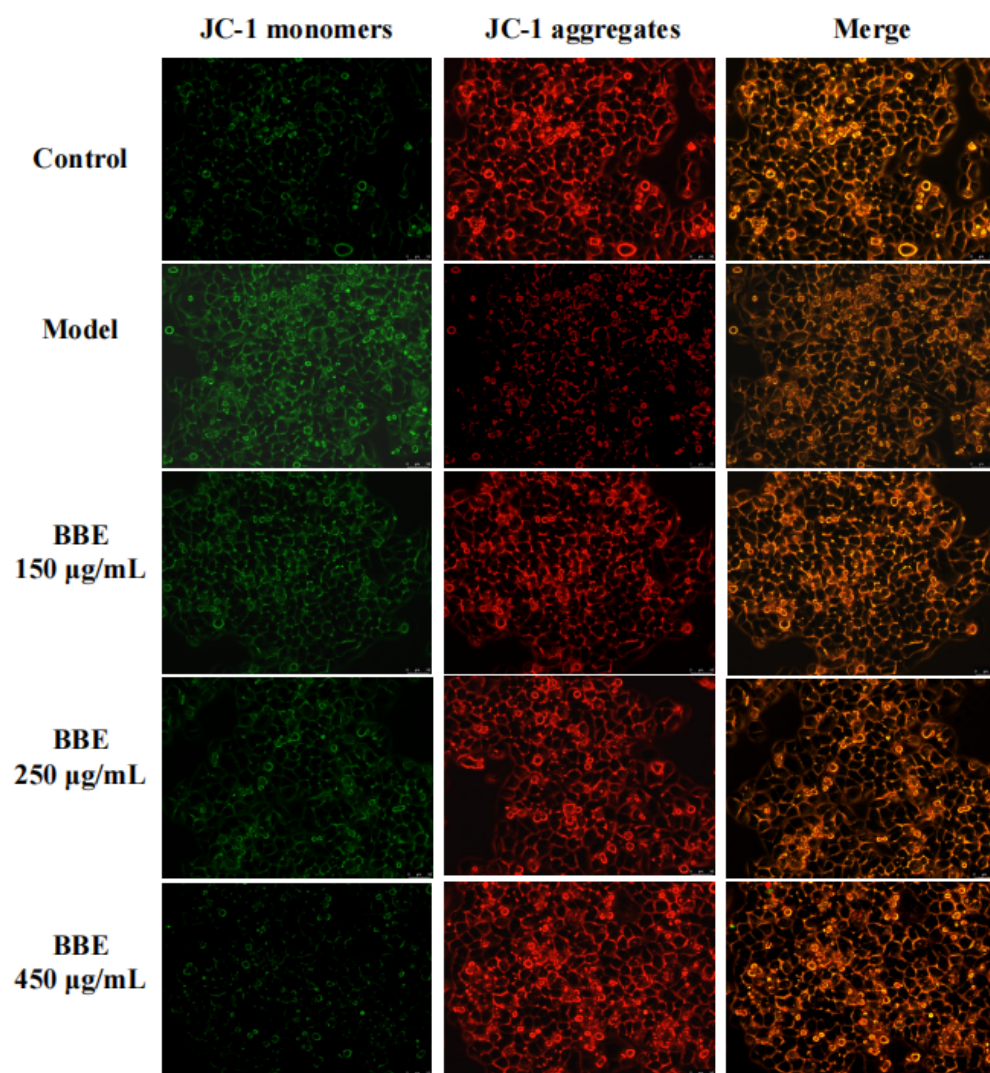


Figure 6. Measurement of mitochondrial membrane potential in HepG2 cells. Cells were stained with JC-1 and visualized on an inverted fluorescence microscope (200× magnification). Red fluorescence of JC-1 dimers was present in the cell areas with high mitochondrial membrane potential, while the green fluorescence of JC-1 monomers was prevalent in the cell areas with low mitochondrial membrane potential.

3.13. Detection of ROS Levels in HepG2 cells

Most polyphenols, flavonoids, and anthocyanins in berries are natural antioxidants. The capacity of blackberry to reduce ethanol-induced oxidative stress was investigated (Figure 7A,B). In HepG2 cells, three BBE treatment groups showed a significant decrease in the production of intracellular ROS initiated by ethanol injury ($p < 0.001$). The strong free radical scavenging activity of BBE could be attributed to its high content of natural antioxidants [22,28]. In this study, after being pre-incubated with BBE, the cells showed significantly relieved ALD-induced oxidative damage and reduced apoptosis. This finding suggested that ROS plays a vital role in ethanol-induced apoptosis and free radical scavenging activity, and BBE could restrain or ease the process. The results coincided with the mitochondrial membrane potential of HepG2 cells.

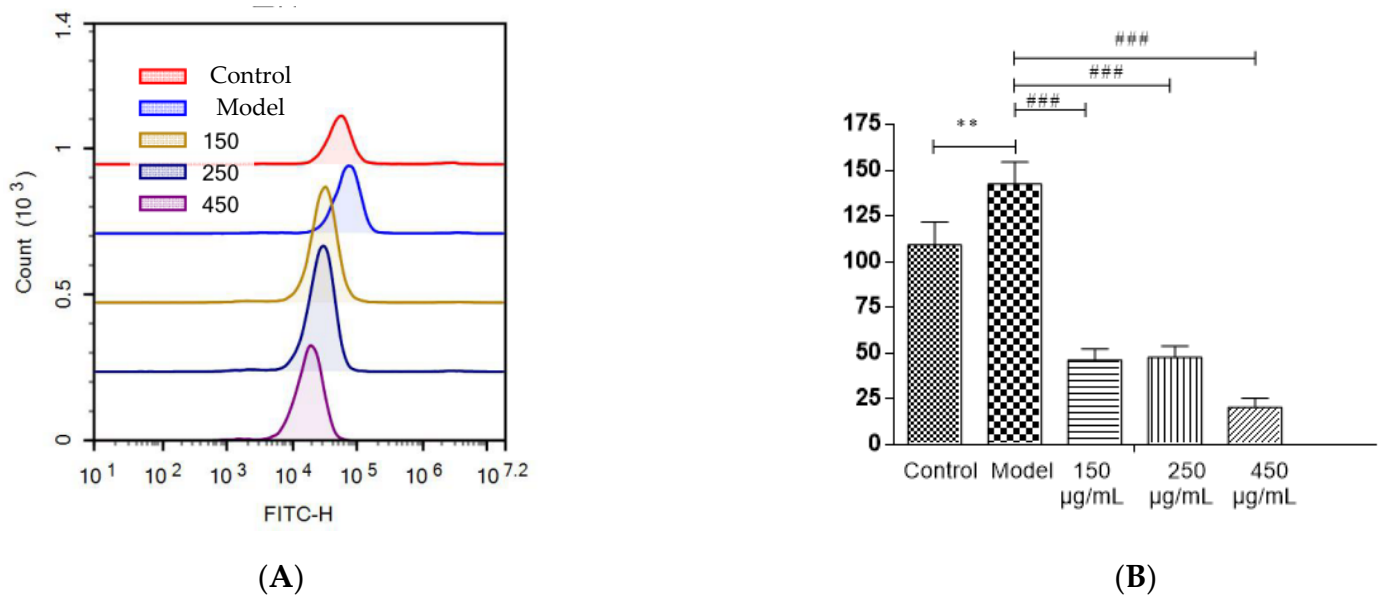
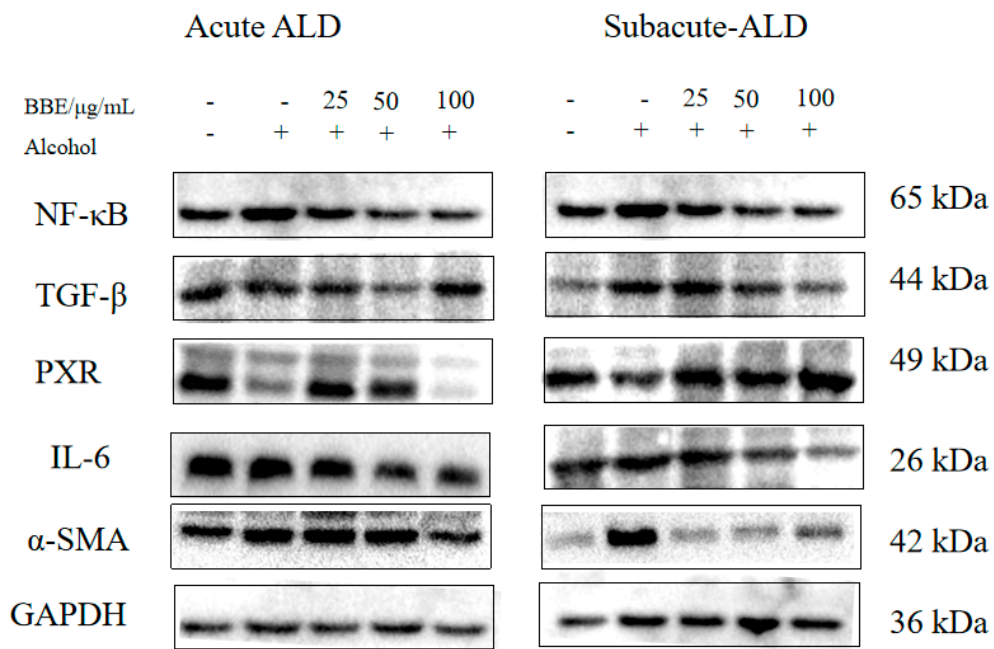


Figure 7. The detection of ROS levels in HepG2 cells (A,B). Values are the mean \pm standard deviation. Compared with control: **, $p < 0.01$. Compared with model: ###, $p < 0.001$.

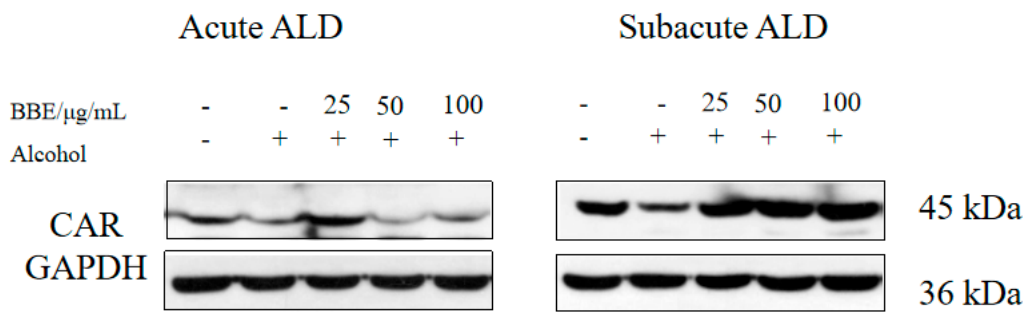
3.14. Western Blotting

Western blotting was used to evaluate the protein expression of NF- κ B, TGF- β , α -SMA, PXR, CAR, and IL-6 in each group to research the effect of BBE on the PXR/PI3K/Akt signaling pathway in the liver (Figure 8A–H). In acute ALD, the expression of NF- κ B, TGF- β , IL-6, and α -SMA ($p < 0.001$) in the model group was higher than those in the control group, whereas the expression of PXR and CAR protein was lower. After BBE was intragastrically administered, the expression of NF- κ B ($p < 0.05$), TGF- β ($p < 0.001$), IL-6 ($p < 0.001$), and α -SMA ($p < 0.01$) in the livers significantly decreased compared with that in the model group, whereas that of PXR ($p < 0.01$, $p < 0.001$) and CAR ($p < 0.001$) significantly increased. In subacute ALD, the trend of protein expression was more obvious than that in acute ALD. The expression of NF- κ B ($p < 0.05$), TGF- β ($p < 0.05$), IL-6 ($p < 0.05$), and α -SMA ($p < 0.001$) in the model group was higher than that in the control group, whereas the expression of PXR ($p < 0.001$) and CAR ($p < 0.05$) protein was lower. After BBE was administered, the expression of NF- κ B ($p < 0.05$, $p < 0.001$, $p < 0.001$), TGF- β ($p < 0.05$, $p < 0.001$, $p < 0.001$), IL-6 ($p < 0.05$, $p < 0.001$, $p < 0.001$), and α -SMA ($p < 0.001$, $p < 0.001$, $p < 0.001$) in the livers significantly decreased compared with that in the model group, whereas the expression of PXR ($p < 0.05$) and CAR ($p < 0.05$, $p < 0.01$, $p < 0.001$) significantly increased. These results suggested that BBE has a good regulatory effect on hepatic metabolic disorder, inflammation, and fibrosis through the PXR-Cytochrome P450s axis.

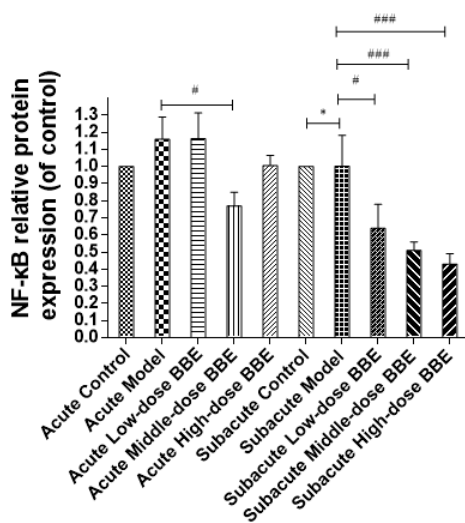
In HepG2 cells, the expression of Bax, a pro-apoptosis protein, decreased ($p < 0.01$, $p < 0.001$), whereas that of PXR ($p < 0.05$, $p < 0.01$) was increased after BBE treatment on ethanol-induced cells. These results indicated that blackberry may prevent cell apoptosis induced by ethanol and elevate the metabolism of alcohol in cells (Figure 8I,J). BBE manifested excellent efficacy in inhibiting liver cell apoptosis through improving the metabolism in liver cells.



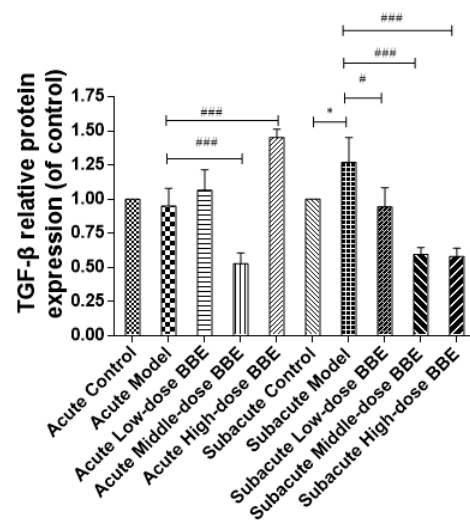
(A)



(B)



(C)



(D)

Figure 8. Cont.

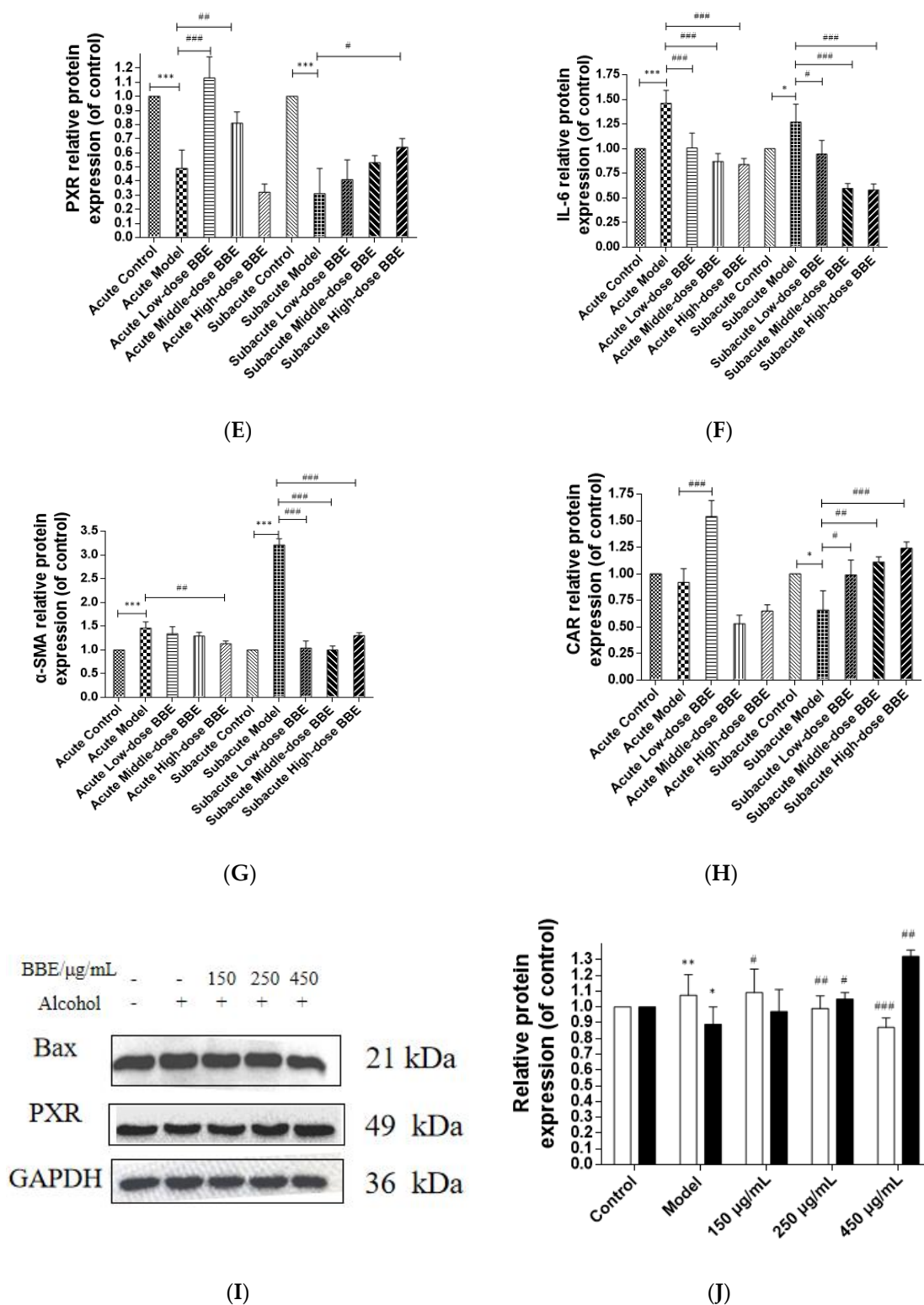


Figure 8. Effects of BBE on the expression of PXR/PI3K/Akt pathways in liver and HepG2 cells (A–J). Western blotting analysis of NF-κB, TGF-β, PXR, IL-6, α-SMA in livers, and the data were normalized to that of GAPDH (A–H), Western blotting analysis of Bax, and PXR in HepG2 cells, and the data were normalized to that of GAPDH (H,I). Values are the mean ± standard deviation. Compared with control: *, $p < 0.05$, **, $p < 0.01$, ***, $p < 0.001$. Compared with model: #, $p < 0.05$, ##, $p < 0.01$. ###, $p < 0.001$.

4. Discussion

Polyphenols are widely distributed in organisms as secondary metabolites. Flavonoids are recognized as natural antioxidants in the diet. Anthocyanins, which are water-soluble pigments, are rich in colored berries, fruits, and vegetables. They prevent high glucose-induced hepatocytes from oxidative damage by improving antioxidant status and inhibiting mitochondrial apoptosis. The mechanism is involved in preventing hyperglycemia-induced mitochondrial depolarization and maintaining its function [31]. In our study, BBE is rich in polyphenols, flavonoids, and anthocyanins. The six main anthocyanins glycosides in nature are cyanidin, followed by delphinidin, peonidin, petunidin, pelargonidin, and malvidin [32]. According to the reports, cyanidin, the main anthocyanin in blackberry fruits, especially cyanidin-3-*O*-glucoside, accounts for more than 80% of total anthocyanins [25].

An increasing number of polyphenols, as natural antioxidants, have attracted the attention of scientists due to their favorable influences on human health. Reactive oxygen and nitrogen species may lead to disastrous consequences, including cancer, cardiovascular disease, diabetes, and neurodegeneration. Polyphenols, which are rich in berries, could eliminate reactive oxygen and nitrogen species and be absorbed from the daily diet or dietary supplementation [33]. BBE is a good natural antioxidant in our study. Several methods, such as DPPH, ABTS, and FRAP, have been frequently utilized to measure the antioxidant capacities of extracts from fresh fruits and vegetables. These assays are simple and practicable, without the need for expensive equipment. However, their principles are different. DPPH and ABTS assays are used to evaluate the free radical scavenging ability of extracts, while the FRAP is used to estimate the electron transfer capacity [34].

Liver injury accounts for liver enlargement, growth retardation, and cirrhosis, and the liver index is an indicator of liver damage [35]. Alcohol retains macromolecules in cells that constitutively secrete protein, triggering increases in liver weights and index in the model group, and finally leading to liver swelling or “balloon”, which is a feature of ALD. Long-term excessive alcohol consumption provokes the decline of appetite and absorption function in mice [36], which apparently results in malnutrition and weight loss [37].

Cellular enzymes, as vital catalysts, play a considerable role in human metabolism [38]. Disorders in lipid metabolism and changes in transaminase activity will occur in ALD. Intemperance severely damages the permeability of cell membranes, and cellular enzymes stored in the liver leak into plasma [39]. ALT, AST, SOD, and MDA levels are essential diagnostic indices of liver function. They are closely related to hepatocyte membrane injury, metabolic syndrome, and hepatic lipid metabolism [40]. The measurement of related indices confirmed these results.

Briefly, 80% alcohol is oxidized and decomposed in the liver after absorption. Heavy drinking causes an imbalance of the antioxidant system and oxidative stress *in vivo*. Persistent oxidative stress could result in liver steatosis, hepatitis, liver fibrosis, liver cirrhosis, and liver cancer [40]. However, ALD usually begins with fatty liver [41]. In our study, the pathological state of the liver treated with BBE was modified in a dose-dependent manner with the observation of H&E staining, Sirius red staining, and oil red O staining.

PXR plays a critical role in the process of exogenous drug metabolism and endogenous lipid and bile acid metabolism [42]. As a nuclear receptor, PXR forms a heterodimer with CAR, enters the nucleus, identifies its corresponding response elements, and finally activates the transcription and expression of its target genes [43]. PXR and CAR regulate the target genes with phase I and phase II drug-metabolizing enzymes and some drug members of the transporter family [44]. CYP3A and CYP2B are phase I-related enzymes of chemical metabolism *in vivo*. CYP3A11, CYP3A25, and CYP2B10 are the main metabolic enzyme genes expressed in mouse hepatocytes.

CYP3A involves the metabolism of more than 50% of clinical drugs, including a large number of hepatotoxic drugs [45,46]. CYP3A4 and CYP3A11 are the most significant subtypes in humans and mice, respectively [47]. Inhibiting these metabolic enzymes could ameliorate ALD. The results of the qRT-PCR analysis indicated that the benefits of BBE in subacute ALD are superior to that in acute ALD. Maybe the reason is that ALD caused

by high-dose ethanol intake may have a devastating effect on liver pathophysiology and lead to multiple organ and system failures [48]. Recovery is also difficult to achieve in a short time. However, the liver damage caused by low-dose ethanol intake is not as severe as that caused by high-dose ethanol. A report revealed that low-dose alcohol intake has a protective effect on the liver to some extent [49].

The development of the reproductive system is significantly affected by the imbalance between cell proliferation and death, such as during folliculogenesis and spermatogenesis [50]. BBE showed a significant protective effect on the ethanol-induced apoptosis of HepG2 cells in our study.

In the reproductive system, oxidative stress is the key pathological basis of liver injury and the major cause of the progression from simple steatosis to steatohepatitis [51]. The imbalance between excessive oxidants and antioxidants gives rise to oxidative stress. In addition, ROS mainly originates from the mitochondria, and antioxidants prevent the organelles from producing ROS to avoid oxidative injury. A large amount of polyphenolic compounds not only directly obliterates reactive species but also indirectly controls the redox environment. Furthermore, multiple cell models showed that polyphenols have the ability to regulate mitochondrial biogenesis and control mitochondrial membrane potential and oxidative phosphorylation [52]. Mitochondrial dysfunction and cellular apoptosis correlate closely with mitochondrial membrane depolarization [53]. In our study, the results indicated that BBE prevents mitochondrial membrane depolarization induced by ethanol. Additionally, BBE, as a natural antioxidant, showed significantly relieved ALD-induced oxidative damage and reduced apoptosis (Figure 9).

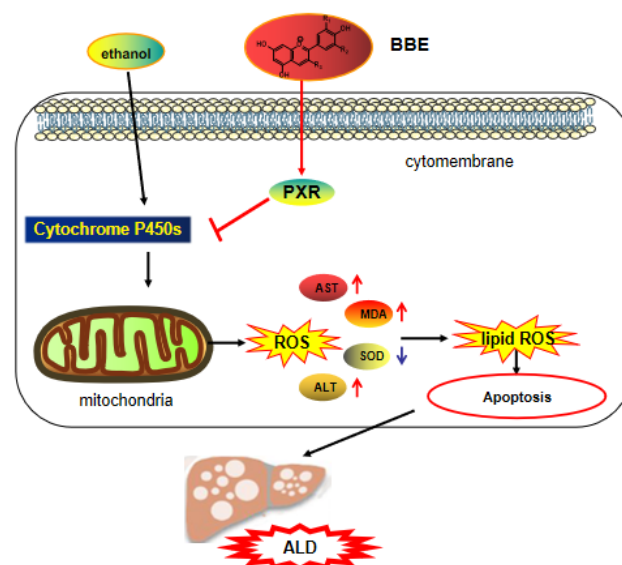


Figure 9. The mechanism of BBE regulating of activating the PXR-Cytochrome P450s axis.

PXR is a ligand-activated transcription factor highly expressed in the liver and gastrointestinal tract [54]. It has the dual identity of xenobiotic sensor and endobiotic receptor for its key role in homeostasis [55], and it plays a vital role in physiological processes, including glucose and lipid metabolism, steroid hormone homeostasis, cholic acid and bilirubin detoxification, bone mineral balance, and immune inflammatory response. The activation of PXR regulates the PI3K/Akt signaling pathway [56], which involves protein synthesis, metabolism, cell cycle regulation, proliferation, and apoptosis [21,57]. This pathway regulates the proliferation and survival of tumor cells and plays a strong part in the process of apoptosis. By inhibiting the PI3K/Akt signaling pathway, many active components of medicinal herbs could mediate cancer cell apoptosis [58].

The pro-apoptotic protein Bax belongs to the Bcl-2 family. It balances the change in $\Delta\Psi_m$, which regulates the intrinsic apoptotic pathway by the mitochondrial apoptotic

pathway [59]. Most drug interaction mechanisms are related to drug metabolism, especially CYP450. The content of the CYP3A4 sub-enzyme is higher than 50% in the liver, which plays an important role in drug metabolism. Recent studies have found that the PXR receptor is the key regulator of CYP3A4 gene transcription, thereby revealing the mechanism of PXR protective effects from exogenous substances at the molecular level. As the “main foreign body receptor”, PXR plays a crucial role in heterologous substances (such as food, drugs, and other components). Alcohol metabolism activates the NF- κ B signaling pathway in the liver and other inflammatory pathways, which lead to the release of a large number of chemokines and inflammatory mediators from damaged hepatocytes and promote the progress of ALD [60]. Additionally, TGF- β is a crucial element involved in liver fibrogenesis [61]. In addition, IL-6 can activate the signal transducer and activator of transcription 3 (STAT3), thereby regulating liver fibrosis and inflammation [62]. α -SMA is a pathological marker of liver fibrosis, for its expression can promote the secretion of ECM in HSC and the progression of liver fibrosis [63,64]. The present study demonstrated that BBE has a good regulatory effect on hepatic metabolic disorder, inflammation, and fibrosis through the PXR-Cytochrome P450s axis, and BBE manifested excellent efficacy in inhibiting liver cell apoptosis through improving the metabolism in liver cells (Figure 9).

5. Conclusions

Alcohol abuse provokes a sharp increase in oxidative stress markers, nutritional disorders, inflammatory response, and histological changes in liver tissue. Heavy drinking is an addictive disease that accounts for hepatitis, fibrosis, cirrhosis, and cancers. As a natural product, blackberry plays an indispensable role in health supplements due to its potential beneficial pharmacological effects. PXR, which could be activated by various compounds, is highly expressed in the liver. Ligand-activated PXR regulates the transcription of a group of genes encoding detoxification-related proteins and transporters involved in metabolite elimination. Therefore, the activation of the PXR-Cytochrome P450s axis is significantly essential for enhancing and accelerating ALD.

In this study, DPPH, ABTS, and FRAP assays showed that BBE has excellent antioxidant activity. The administration of BBE could extensively decrease the biochemical parameters of ALT, AST, MDA, and SOD *in vivo*. These results suggested the protective effect of BBE on ALD, as confirmed by liver indices and histopathological observation, including H&E staining, oil red O staining, and Sirius red staining. Network analysis and docking studies revealed that BBE improved apoptosis via the PI3K-Akt signaling pathway, which has a preventive effect on ALD. Furthermore, Western blot and qRT-PCR results proved that BBE regulated liver metabolic disorder, inflammation, and fibrosis in ALD models. This study demonstrated the protective effect of BBE on ALD for the first time. The protective mechanisms may be attributed to the strong antioxidant activities of its anthocyanins. In addition, ethanol-induced HepG2 cells as a model of ALD *in vitro* showed that BBE improved apoptosis in a dose-dependent manner, which was consistent with the mitochondrial membrane potential of HepG2 cells. BBE also significantly reduced ALD-induced oxidative damage and apoptosis by down-regulating the ROS content and Bax protein expression and up-regulating the PXR level. The amelioration of ALD by blackberry is in connection with activating the PXR-Cytochrome P450s axis (Figure 9). This study provides a new and promising natural product for the treatment of alcoholic liver injury.

Supplementary Materials: The following supporting information can be downloaded at: <https://www.mdpi.com/article/10.3390/separations9100321/s1>, Figure S1: Network pharmacology Diagram of Cyanidin-3-O-glucoside. (A) Related targets of cyanidin-3-O-glucoside, the green circular and red polygons respectively represented cyanidin-3-O-glucoside-targeted genes and cyanidin-3-O-glucoside. (B) Venn map of cyanidin-3-O-glucoside target and ALD target; Table S1: Shared target information of cyanidin-3-O-glucoside; Figure S2: PPI network of the intersection target of cyanidin-3-O-glucoside for ALD; Figure S3: Histogram of Go analysis of cyanidin-3-O-glucoside (A) The enriched terms in biological process (BP); (B) The enriched terms in cellular component

(CC); (C) The enriched terms in molecular function (MF); Figure S4: KEGG pathway diagram of cyanidin-3-O-glucoside; Figure S5: “Component-target-pathway-disease” network diagram.

Author Contributions: T.X.: Conceptualization, Methodology, Investigation, Project administration, Validation, Visualization, Writing—original draft. Z.G.: Formal analysis, Resources, investigation, Writing—review and editing. M.F.: Resources, Data curation. J.H. and X.W.: Resources, funding acquisition. Y.Z. and L.T.: Resources. X.S.: Methodology, Visualization, Resources, Supervision, Writing—review and editing. All authors have read and agreed to the published version of the manuscript.

Funding: This research was supported by a grant from the Basic Scientific Research Project of Guizhou Province (grant number [2021] 535), the Doctoral Fund of Guizhou Medical University (grant number [2018] 013), the Fund of Science and Technology Project of Guizhou provincial health commission (gzwjkj 2019-1-181), the Guizhou Medical University Breeding programs of National Natural Science Foundation of China (grant number 19NSP074).

Institutional Review Board Statement: The experiments were conducted according to the guidelines of the Declaration of Helsinki and were approved by the Institutional Review Board (or Ethics Committee) of Guizhou Medical University. All animal operating procedures obey the regulations on animal experiments issued by the National Science and Technology Commission of the People’s Republic of China and the guidelines for the care and use of laboratory animals issued by the National Institutes of Health (Experimental facility certification No.: SYXK (Guizhou) 2018-0001).

Informed Consent Statement: Not applicable.

Data Availability Statement: Data are contained within the manuscript and Supplementary Materials.

Conflicts of Interest: The authors declare no conflict of interest.

Abbreviations

PXR, pregnane X receptor; ALD, alcoholic liver disease; P450, cytochrome P450 oxidase; AST, aspartate aminotransferase; alanine aminotransferase; SOD, superoxide dismutase; MDA, malondialdehyde; BBE, extract of blackberry; NF- κ B, nuclear factor kappa-B; TGF- β , transforming growth factor- β ; IL-6, interleukin- 6; CAR, constitutive androstane receptor; CYP3A25, cytochrome P450-3A25; CYP3A11, cytochrome P450-3A11; CYP2B10-cytochrome P450-2B10; IARC, international agency for research on cancer; NRs, nuclear receptors; RXR α , retinoid X receptor alpha; DPPH, 2,2-diphenyl-1-picrylhydrazyl; ABTS, 3-ethyl- benzothiazoline-6-sulfonic acid; TPTZ, 2,4,6-tris(2-pyridyl)-s-triazine; V_C, ascorbic acid; TPC, total phenolic content; TFC, total flavonoids content; TMA, total anthocyanin content; FRAP, ferric reducing antioxidant power; CMC, carboxymethylcellulose; BW, body weight; PPI, protein protein interaction; GO, gene ontology; KEGG, Kyoto Encyclopedia of Genes and Genomes; MF, molecular function; BP, biological process; CC, cellular component; RT-PCR, reverse transcription-polymerase chain reaction; DMSO, dimethylsulfoxide; DMEM, dulbecco’s modified eagle medium; DHE, dihydroethidium; SDS-PAGE, sodium dodecyl sulfate polyacrylamide gel electrophoresis.

References

1. Justice, A.C. Alcohol and the global burden of cancer: What are we missing? *Lancet Oncol.* **2021**, *22*, 1048–1049. [[CrossRef](#)]
2. Li, Y.G.; Ji, D.F.; Zhong, S.; Shi, L.G.; Hu, G.Y.; Chen, S. Saponins from *Panax japonicus* Protect against Alcohol-Induced Hepatic Injury in Mice by Up-regulating the Expression of GPX3, SOD1 and SOD3. *Alcohol Alcohol.* **2010**, *45*, 320–331. [[CrossRef](#)]
3. Rattan, P.; Shah, V.H. Review article: Current and emerging therapies for acute alcohol-associated hepatitis. *Aliment. Pharmacol. Ther.* **2022**, *56*, 28–40. [[CrossRef](#)]
4. Lee, D.U.; Chou, H.; Wang, E.; Fan, G.H.; Han, J.; Chang, K.; Kwon, J.; Lee, K.J.; Blanchard, J.; Urrunaga, N.H. The clinical implication of psychiatric illnesses in patients with alcoholic liver disease: An analysis of US hospitals. *Expert Rev. Gastroenterol. Hepatol.* **2022**, *16*, 689–697. [[CrossRef](#)]
5. Singal, A.K.; Arsalan, A.; Dunn, W.; Arab, J.P.; Wong, R.J.; Kuo, Y.F.; Kamath, P.S.; Shah, V.H. Alcohol-associated liver disease in the United States is associated with severe forms of disease among young, females and Hispanics. *Aliment. Pharmacol. Ther.* **2021**, *54*, 451–461. [[CrossRef](#)] [[PubMed](#)]

6. Wu, S.; Yue, Y.; Tian, H.; Li, X.; He, W.; Ding, H. Carthamus red from *Carthamus tinctorius* L. exerts antioxidant and hepatoprotective effect against CCl₄-induced liver damage in rats via the Nrf2 pathway. *J. Ethnopharmacol.* **2013**, *148*, 570–578. [[CrossRef](#)]
7. Potts, J.R.; Goubet, S.; Heneghan, M.A.; Verma, S. Determinants of long-term outcome in severe alcoholic hepatitis. *Aliment. Pharmacol. Ther.* **2013**, *38*, 584–595. [[CrossRef](#)] [[PubMed](#)]
8. Thursz, M.R.; Richardson, P.; Allison, M.; Austin, A.; Bowers, M.; Day, C.P.; Downs, N.; Gleeson, D.; Macgilchrist, A.; Grant, A.; et al. Prednisolone or pentoxifylline for alcoholic hepatitis. *New Engl. J. Med.* **2015**, *372*, 1619–1628. [[CrossRef](#)]
9. Plauth, M.; Bernal, W.; Dasarathy, S.; Merli, M.; Plank, L.D.; Schütz, T.; Bischoff, S. ESPEN guideline on clinical nutrition in liver disease. *Clin. Nutr.* **2019**, *38*, 485–521. [[CrossRef](#)]
10. Petrasek, J.; Bala, S.; Csak, T.; Lippai, D.; Kodys, K.; Menashy, V.; Barrieau, M.; Min, S.; Kurt-Jones, E.A.; Szabo, G. IL-1 receptor antagonist ameliorates inflammasome-dependent alcoholic steatohepatitis in mice. *J. Clin. Invest.* **2012**, *122*, 3476–3489. [[CrossRef](#)] [[PubMed](#)]
11. Aghemo, A.; Alekseeva, O.P.; Angelico, F.; Bakulin, I.G.; Bakulina, N.V.; Bordin, D.; Bueverov, A.O.; Drapkina, O.M.; Gillessen, A.; Kagarmanova, E.M.; et al. Role of silymarin as antioxidant in clinical management of chronic liver diseases: A narrative review. *Ann. Med.* **2022**, *54*, 1548–1560. [[CrossRef](#)] [[PubMed](#)]
12. Zhang, B.; Xie, W.; Krasowski, M.D. PXR: A xenobiotic receptor of diverse function implicated in pharmacogenetics. *Pharmacogenomics* **2008**, *9*, 1695–1709. [[CrossRef](#)] [[PubMed](#)]
13. Oladimeji, P.O.; Chen, T. PXR: More than just a master xenobiotic receptor. *Mol. Pharmacol.* **2018**, *93*, 119–127. [[CrossRef](#)]
14. Ghareaghajlou, N.; Hallaj-Nezhadi, S.; Ghasempour, Z. Red cabbage anthocyanins: Stability, extraction, biological activities and applications in food systems. *Food Chem.* **2021**, *365*, 130482. [[CrossRef](#)]
15. Fernández-Demeneghi, R.; Rodríguez-Landa, J.; Guzmán-Gerónimo, R.; Acosta-Mesa, H.; Meza-Alvarado, E.; Vargas-Moreno, I.; Herrera-Meza, S. Effect of blackberry juice (*Rubus fruticosus* L.) on anxiety-like behaviour in Wistar rats. *Int. J. Food Sci. Nutr.* **2019**, *70*, 856–867. [[CrossRef](#)] [[PubMed](#)]
16. Kim, H.; Jeong, D.; Kim, S.; Lee, S.; Sin, H.; Yu, K.; Jeong, S.; Kim, S. Fermentation of Blackberry with *L. plantarum* JBMI F5 Enhance the Protection Effect on UVB-Mediated Photoaging in Human Foreskin Fibroblast and Hairless Mice through Regulation of MAPK/NF- κ B Signaling. *Nutrients* **2019**, *11*, 2429. [[CrossRef](#)] [[PubMed](#)]
17. Figueira, I.; Tavares, L.; Jardim, C.; Costa, I.; Terrasso, A.P.; Almeida, A.F.; Santo, C.N. Blood-brain barrier transport and neuroprotective potential of blackberry-digested polyphenols: An in vitro study. *Eur. J. Nutr.* **2019**, *58*, 113–130. [[CrossRef](#)]
18. Cenk, E.; Schmutz, C.; Pahlke, G.; Oertel, A.; Kollarova, J.; Mock, H.P.; Matros, A.; Marko, D. Immunomodulatory Properties of blackberry anthocyanins in THP-1 derived macrophages. *Int. J. Mol. Sci.* **2021**, *22*, 10483. [[CrossRef](#)]
19. Tatar, M.; Bagheri, Z.; Varedi, M.; Naghibalhossaini, F. Blackberry extract inhibits telomerase activity in human colorectal cancer cells. *Nutrition Cancer Int. J.* **2019**, *71*, 461–471. [[CrossRef](#)]
20. Wang, Y.; Zhao, Y.; Wang, D.; Huo, Y.; Ji, B. Anthocyanin-rich extracts from blackberry, wild blueberry, strawberry, and chokeberry: Antioxidant activity and inhibitory effect on oleic acid-induced hepatic steatosis in vitro. *Int. J. Food Sci. Nutr.* **2016**, *96*, 2494–2503. [[CrossRef](#)]
21. Xiao, T.; Luo, Z.; Guo, Z.; Wang, X.; Ding, M.; Wang, W.; Shen, X.; Zhao, Y. Multiple Roles of Black Raspberry Anthocyanins Protecting against Alcoholic Liver Disease. *Molecules* **2021**, *26*, 2313. [[CrossRef](#)] [[PubMed](#)]
22. Xiao, T.; Guo, Z.; Sun, B.; Zhao, Y. Identification of Anthocyanins from Four Kinds of Berries and Their Inhibition Activity to α -Glycosidase and Protein Tyrosine Phosphatase 1B by HPLC FT-ICR MS/MS. *J. Agric. Food Chem.* **2017**, *65*, 6211–6221. [[CrossRef](#)] [[PubMed](#)]
23. Zheng, J.; Zheng, X.; Zhao, L.; Yi, J.; Cai, S. Effects and interaction mechanism of soybean 7S and 11S globulins on anthocyanin stability and antioxidant activity during in vitro simulated digestion. *Curr. Res. Food Sci.* **2021**, *4*, 543–550. [[CrossRef](#)] [[PubMed](#)]
24. Zhang, G.; Wang, H.; Zhu, K.; Yang, Y.; Li, J.; Jiang, H.; Liu, Z. Investigation of candidate molecular biomarkers for expression profile analysis of the Gene expression omnibus (GEO) in acute lymphocytic leukemia (ALL). *Biomed. Pharm.* **2019**, *120*, 109530. [[CrossRef](#)] [[PubMed](#)]
25. Jakobek, L.; Seruga, M.; Medvidovic-Kosanovic, M.; Novak, I. Anthocyanin content and antioxidant activity of various red fruit juices. *Dtsch. Lebensm. Rundsch.* **2007**, *103*, 58–64.
26. Cho, M.J.; Howard, L.R.; Prior, R.L.; Clark, J.R. Flavonoid glycosides and antioxidant capacity of various blackberry, blueberry and red grape genotypes determined by high-performance liquid chromatography/mass spectrometry. *J. Sci. Food Agric.* **2004**, *84*, 1771–1782. [[CrossRef](#)]
27. Zhao, H.; Wu, W.; Lü, L.; Li, W. Change Regularity of Polyphenol Content in Blackberry Fruit during Growth and Development. *J. Jilin Agric. Univ.* **2013**, *35*, 457–462.
28. Xiao, T.; Guo, Z.; Bi, X.; Zhao, Y. Polyphenolic profile as well as anti-oxidant and anti-diabetes effects of extracts from freeze-dried black raspberries. *J. Funct. Foods* **2017**, *31*, 179–187. [[CrossRef](#)]
29. Sozio, M.; Crabb, D.W. Alcohol and lipid metabolism. *Am. J. Physiol. Endocrinol. Metab.* **2008**, *295*, E10–E16. [[CrossRef](#)]
30. Li, S.; Fan, T.P.; Jia, W.; Lu, A.; Zhang, W. Network Pharmacology in Traditional Chinese Medicine. *Evid. Based Complement. Altern. Med.* **2014**, *2014*, 138460. [[CrossRef](#)]

31. Jiang, X.; Tang, X.; Zhang, P.; Liu, G.; Guo, H. Cyanidin-3-O-b-glucoside protects primary mouse hepatocytes against high glucose-induced apoptosis by modulating mitochondrial dysfunction and the PI3K/Akt pathway. *Biochem. Pharmacol.* **2014**, *90*, 135–144. [[CrossRef](#)] [[PubMed](#)]
32. Prior, R.L.; Wu, X. Anthocyanins: Structural characteristics that result in unique metabolic patterns and biological activities. *Free Radic. Res.* **2006**, *40*, 1014–1028. [[CrossRef](#)] [[PubMed](#)]
33. Nakamura, T.; Lipton, S.A. Preventing Ca²⁺-mediated nitrosative stress in neurodegenerative diseases: Possible pharmacological strategies. *Cell Calcium* **2010**, *47*, 190–197. [[CrossRef](#)] [[PubMed](#)]
34. Thaipong, K.; Boonprakob, U.; Crosby, K.; Cisneros-Zevallos, L.; Byrne, D.H. Comparison of ABTS, DPPH, FRAP, and ORAC assays for estimating antioxidant activity from guava fruit extracts. *J. Food Compos. Anal.* **2006**, *19*, 669–675. [[CrossRef](#)]
35. Xiang, J.; Zhu, W.; Li, Z.; Ling, S. Effect of juice and fermented vinegar from *Hovenia dulcis* peduncles on chronically alcohol induced liver damage in mice. *Food Funct.* **2012**, *3*, 628–634. [[CrossRef](#)] [[PubMed](#)]
36. Lieber, C.S. Alcoholic fatty liver: Its pathogenesis and mechanism of progression to inflammation and fibrosis. *Alcohol* **2004**, *34*, 9–19. [[CrossRef](#)] [[PubMed](#)]
37. Wu, W.; Chen, J.; Liu, C.; Kong, P.; Yan, J.; Cheng, H. Protective Effect of Green Tea Polyphenols against Chronic Alcoholic Hepatic Injury in Mice. *Food Sci.* **2011**, *32*, 310–313.
38. He, Z.; Wang, Y.; Liu, L.; Lou, Z. Effects of Panax Japonicus Extractions on Serum Biochemical Indices and Inflammatory Factors in Mice with Alcoholic Liver Injury. *Zhejiang J. Integr. Tradit. Chin. West. Med.* **2018**, *28*, 21–24.
39. Baldi, E.; Burra, P.; Plebani, M.; Salvagnini, M. Serum malondialdehyde and mitochondrial aspartate aminotransferase activity as markers of chronic alcohol intake and alcoholic liver disease. *Ital. J. Gastroenterol. Hepatol.* **1993**, *25*, 429–432.
40. Sun, H.; Mu, T.; Liu, X.; Zhang, M.; Chen, J. Purple sweet potato (*Lpomoëa batatas* L.) anthocyanins: Preventive effect on acute and subacute alcoholic liver damage and dealcoholic effect. *J. Agric. Food Chem.* **2014**, *62*, 2364–2373. [[CrossRef](#)]
41. Yang, C.; Liao, A.; Cui, Y.; Yu, G.; Hou, Y.; Pan, L.; Chen, W.; Zheng, S.; Li, X.; Ma, J.; et al. Wheat embryo globulin protects against acute alcohol-induced liver injury in mice. *Food Chem. Toxicol.* **2021**, *153*, 112240. [[CrossRef](#)] [[PubMed](#)]
42. Zeng, H.; Jiang, Y.; Chen, P.; Fan, X.; Li, D.; Liu, A.; Ma, X.; Xie, W.; Liu, P.; Gonzalez, F.J.; et al. Schisandrol B protects against cholestatic liver injury through pregnane X receptors. *Br. J. Pharmacol.* **2017**, *174*, 672–688. [[CrossRef](#)] [[PubMed](#)]
43. Ostberg, T.; Bertilsson, G.; Jendeberg, L.; Berkenstam, A.; Uppenberg, J. Identification of residues in the PXR ligand binding domain critical for species specific and constitutive activation. *Eur. J. Biochem.* **2002**, *269*, 4896–4904. [[CrossRef](#)] [[PubMed](#)]
44. Jia, Y.; Viswakarma, N.; Reddy, J.K. Med1 subunit of the mediator complex in nuclear receptor-regulated energy metabolism, liver regeneration, and hepatocarcinogenesis. *Gene Expr.* **2014**, *16*, 63–75. [[CrossRef](#)]
45. Wilkinson, G.R. Cytochrome P4503A (CYP3A) metabolism: Prediction of in vivo activity in humans. *J. Pharmacokinet. Biopharm.* **1996**, *24*, 475–490. [[CrossRef](#)]
46. Jones, B.C.; Rollison, H.; Johansson, S.; Kanebratt, K.P.; Lambert, C.; Vishwanathan, K.; Andersson, T.B. Managing the risk of CYP3A induction in drug development: A strategic approach. *Drug Metab. Dispos.* **2017**, *45*, 35–41. [[CrossRef](#)]
47. Komura, H.; Iwaki, M. Species differences in in vitro and in vivo small intestinal metabolism of CYP3A substrates. *J. Pharm. Sci.* **2008**, *97*, 1775–1800. [[CrossRef](#)] [[PubMed](#)]
48. Christidis, C.; Karatayli, E.; Hall, R.A.; Weber, S.N.; Reichert, M.C.; Hohl, M.; Qiao, S.; Boehm, U.; Lütjohann, D.; Lammert, F.; et al. Fibroblast Growth Factor 21 Response in a Preclinical Alcohol Model of Acute-on-Chronic Liver Injury. *Int. J. Mol. Sci.* **2021**, *22*, 7898. [[CrossRef](#)] [[PubMed](#)]
49. Liu, F.; Yu, H.; Liao, C.; Chou, A.; Lee, H. The Timing and Effects of Low-Dose Ethanol T treatment on Acetaminophen-Induced Liver Injury. *Life* **2021**, *11*, 1094. [[CrossRef](#)]
50. Larsen, B.D.; Sørensen, C.S. The caspase-activated DNase: Apoptosis and beyond. *FEBS J.* **2017**, *284*, 1160–1170. [[CrossRef](#)]
51. Sumida, Y.; Niki, E.; Naito, Y.; Yoshikawa, T. Involvement of free radicals and oxidative stress in NAFLD/NASH. *Free Radic. Res.* **2013**, *47*, 869–880. [[CrossRef](#)] [[PubMed](#)]
52. Serrano, J.C.; Cassanye, A.; Martín-Gari, M.; Granado-Serrano, A.B.; Portero-Otín, M. Effect of dietary bioactive compounds on mitochondrial and metabolic flexibility. *Diseases* **2016**, *4*, 14. [[CrossRef](#)]
53. Fulda, S. Modulation of mitochondrial apoptosis by PI3K inhibitors. *Mitochondrion* **2013**, *13*, 195–198. [[CrossRef](#)]
54. Handschin, C.; Podvinec, M.; Meyer, U.A. CXR, a chicken xenobiotic-sensing orphan nuclear receptor, is related to both mammalian pregnane X receptor (PXR) and constitutive androstane receptor (CAR). *Proc. Natl. Acad. Sci. USA* **2000**, *97*, 10769–10774. [[CrossRef](#)]
55. Garcia, M.; Thirouard, L.; Sedes, L.; Monroe, M.; Holota, H.; Caira, F.; Volle, D.H.; Beaudoin, C. Nuclear receptor metabolism of bile acids and xenobiotics: A coordinated detoxification system with impact on health and diseases. *Int. J. Mol. Sci.* **2018**, *19*, 3630. [[CrossRef](#)] [[PubMed](#)]
56. Luan, Z.; Wei, Y.; Huo, X.; Sun, X.; Zhang, C.; Ming, W.; Luo, Z.; Du, C.; Li, Y.; Xu, H.; et al. Pregnane X receptor (PXR) protects against cisplatin-induced acute kidney injury in mice. *BBA-Mol. Basis Dis.* **2021**, *1867*, 165996. [[CrossRef](#)]
57. Yan, W.; Ma, X.; Zhao, X.; Zhang, S. Baicalein induces apoptosis and autophagy of breast cancer cells via inhibiting PI3K/AKT pathway in vivo and vitro. *Drug Des. Dev. Ther.* **2018**, *12*, 3961–3972. [[CrossRef](#)]
58. Feng, L.-X.; Sun, P.; Mi, T.; Liu, M.; Liu, W.; Yao, S.; Cao, Y.-M.; Yu, X.-L.; Wu, W.-Y.; Jiang, B.-H. Agglutinin isolated from *Arisema heterophyllum* Blume induces apoptosis and autophagy in A549 cells through inhibiting PI3K/Akt pathway and inducing ER stress. *Chin. J. Nat. Med.* **2016**, *14*, 856–864. [[CrossRef](#)]

59. Gu, X.; Yao, Y.; Cheng, R.; Zhang, Y.; Dai, Z.; Wan, G.; Yang, Z.; Cai, W.; Gao, G.; Yang, X. Plasminogen K5 activates mitochondrial apoptosis pathway in endothelial cells by regulating Bak and Bcl-xL subcellular distribution. *Apoptosis* **2011**, *16*, 846–855. [[CrossRef](#)]
60. Zhao, N.; Xia, G.; Cai, J.; Li, Z.; Lv, X. Adenosine receptor A2B mediates alcoholic hepatitis by regulating cAMP levels and the NF-KB pathway. *Toxicol. Lett.* **2022**, *359*, 84–95. [[CrossRef](#)] [[PubMed](#)]
61. Kartasheva-Ebertz, D.; Gaston, J.; Lair-Mehiri, L.; Massault, P.; Scatton, O.; Vaillant, J.; Morozov, V.-A.; Pol, S.; Lagaye, S. Adult human liver slice cultures: Modelling of liver fibrosis and evaluation of new anti-fibrotic drugs. *World J. Hepatol.* **2021**, *13*, 187–217. [[CrossRef](#)] [[PubMed](#)]
62. Al-Humadi, H.-W.; Al-Saigh, R.; Sahib, A. The impact of low alcohol consumption on the liver and inflammatory cytokines in diabetic rats. *Adv. Clin. Exp. Med.* **2019**, *28*, 331–337. [[CrossRef](#)] [[PubMed](#)]
63. Ramachandran, P.; Unny, A.K.; Vij, M.; Safwan, M.; Balaji, M.S.; Rela, M. α -Smooth muscle actin expression predicts the outcome of Kasai portoenterostomy in biliary atresia. *Saudi J. Gastroenterol.* **2019**, *25*, 101–105. [[CrossRef](#)]
64. Roehlen, N.; Crouchet, E.; Baumert, T.F. Liver fibrosis: Mechanistic concepts and therapeutic perspectives. *Cells* **2020**, *9*, 875. [[CrossRef](#)]